

# Octupole deformation in the ground states of even-even nuclei: a global analysis within the covariant density functional theory.

S. E. Agbemava,<sup>1</sup> A. V. Afanasjev,<sup>1</sup> and P. Ring<sup>2</sup>

<sup>1</sup>*Department of Physics and Astronomy, Mississippi State University, MS 39762*

<sup>2</sup>*Fakultät für Physik, Technische Universität München, D-85748 Garching, Germany*

(Dated: March 11, 2016)

A systematic investigation of octupole deformed nuclei is presented for even-even systems with  $Z \leq 106$  located between the two-proton and two-neutron drip lines. For this study we use five most up-to-date covariant energy density functionals of different types, with a non-linear meson coupling, with density dependent meson couplings, and with density-dependent zero-range interactions. Pairing correlations are treated within relativistic Hartree-Bogoliubov (RHB) theory based on an effective separable particle-particle interaction of finite range. This allows us to assess theoretical uncertainties within the present covariant models for the prediction of physical observables relevant for octupole deformed nuclei. In addition, a detailed comparison with the predictions of non-relativistic models is performed. A new region of octupole deformation, centered around  $Z \sim 98, N \sim 196$  is predicted for the first time. In terms of its size in the  $(Z, N)$  plane and the impact of octupole deformation on binding energies this region is similar to the best known region of octupole deformed nuclei centered at  $Z \sim 90, N \sim 136$ . For the later island of octupole deformed nuclei, the calculations suggest substantial increase of its size as compared with available experimental data.

PACS numbers: 21.60.Jz, 21.10.Dr, 21.10.Ft, 21.10.Gv

## I. INTRODUCTION

Reflection asymmetric (or octupole deformed) shapes represent an interesting example of symmetry breaking of the nuclear mean field. The physics of such shapes in the normal deformed minimum (both in non-rotating and rotating systems) has been extensively studied in the 80ies and 90ies of the last century (see the review in Ref. [1]). Reflection asymmetric shapes are also present for large deformations at the outer fission barriers in the actinides, superheavy nuclei and nuclei important in the r-process of nucleosynthesis [1–3]. At present, there is a revival of the interest to the study of such shapes. It is seen in a substantial number of theoretical [4–17] and experimental [18–26] studies of octupole correlations and octupole deformed nuclei in the normal deformed minimum. Moreover, the attempts to understand microscopically the fission process, cluster radioactivity and the stability of superheavy elements [2, 27–37] as well as renewed interest to experimental studies of fission [38–40] created a substantial interest in octupole deformed shapes at large deformations.

The existence of octupole deformed shapes is dictated by the underlying shell structure. Strong octupole coupling exists for particle numbers associated with a large  $\Delta N = 1$  interaction between intruder orbitals with  $(l, j)$  and normal-parity orbitals with  $(l - 3, j - 3)$  [1]. For normal deformed nuclei not far away from beta stability the tendency towards octupole deformation or strong octupole correlations occurs just above closed shells at particle numbers near 34 (the coupling between the  $1g_{9/2}$  and  $2p_{3/2}$  orbitals), 56 (the coupling between the  $1h_{11/2}$  and  $2d_{5/2}$  orbitals), 88 (the coupling between the  $1i_{13/2}$  and  $2f_{7/2}$  orbitals) and 134 (the coupling between the  $1j_{15/2}$  and  $2g_{9/2}$  orbitals) [1].

Some of the studies of the octupole shapes have been performed in the framework of covariant density functional theory (CDFT) [41]. Built on Lorentz covariance and the Dirac equation, CDFT provides a natural incorporation of spin degrees of freedom [42, 43] and a good parameter free description of spin-orbit splittings [43–45], which have an essential influence on the underlying shell structure. In CDFT the time-odd components of the mean fields are given by the spatial components of the Lorentz vectors. Therefore, because of Lorentz invariance, these fields are coupled with the same constants as the time-like components [46] which are fitted in time-even systems to ground state properties of finite nuclei.

The first investigation of the role of octupole deformation in the CDFT framework has been performed in Ref. [47]. In this work, the occurrence of stable octupole deformation in the ground states of the Ra isotopes and the impact of octupole deformation on fission barriers of the  $^{226}\text{Ra}$ ,  $^{232}\text{Th}$  and  $^{240}\text{Pu}$  nuclei has been studied with the covariant energy density functionals (CEDFs) NL1, NLSH and PL-40. However, because of some deficiencies these functionals are no longer in use. During the last ten years some extra calculations for the ground states of octupole deformed nuclei have been performed in the Ra [13, 48], Th [12, 13], Ba [13, 49] and Sm [13, 50] isotope chains. The choice of these nuclei have been motivated by the results of the analysis of experimental data performed in non-relativistic theories.

However, a number of questions are left beyond the scope of these investigations. First of them is related to a global survey of octupole deformed and octupole soft nuclei in the CDFT framework across the full nuclear landscape. As mentioned above, existing CDFT studies are very limited in scope. On the contrary, more systematic surveys of octupole deformed nuclei exist in

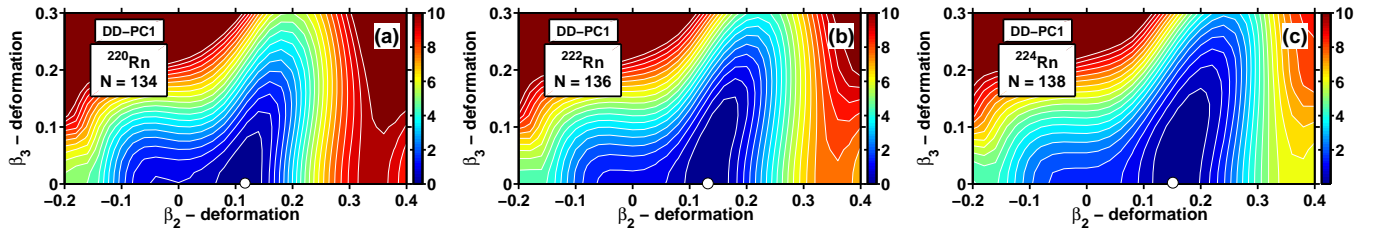


FIG. 1. (Color online) Potential energy surfaces of the Rn isotopes in the  $(\beta_2, \beta_3)$  plane calculated with the CEDF DD-PC1. The white circle indicates the global minimum. Equipotential lines are shown in steps of 0.5 MeV. The neutron number  $N$  is shown in each panel in order to make the comparison between different isotones easier.

non-relativistic models [6, 51]. The results of the macroscopic+microscopic (MM) approach of Ref. [51] cover all nuclei with  $Z \leq 108$  from the proton-drip line up to  $N = 160$ . On the contrary, the non-relativistic Hartree-Fock-Bogoliubov (HFB) studies with the Gogny force [6] cover only regions of known nuclei.

The second question is related to the estimate of theoretical uncertainties in the description of octupole deformed nuclei. The importance of such estimate become clear in the light of recent publications [52–56]. However, theoretical uncertainties in the description of octupole deformed nuclei have not been studied so far. Such an estimate is not possible based on the results of previous studies since they were performed either with only one functional (PK1 in Ref. [50] for Sm isotopes, NL1 and NL3 in Ref. [48] for  $^{226}\text{Ra}$ , DD-PC1 in [12, 13] for Th, Ra, Sm, and Ba isotopes) or the studies for a given nucleus or isotope chain have been performed in different frameworks (relativistic mean field plus BCS (RMF+BCS) in Refs. [48–50] versus relativistic Hartree Bogoliubov (RHB) in Refs. [12, 13]) using different prescriptions for the pairing interaction. In addition, the choice of nuclei in these studies is quite limited (not exceeding six nuclei per isotope chain).

To address these two questions, we have performed a global survey of all even-even  $Z \leq 106$  nuclei located between the two-proton and two-neutron drip lines employing the DD-PC1 [57] and NL3\* [58] CEDFs. Additional studies with the DD-ME2 [59], PC-PK1 [60] and DD-ME $\delta$  [61] functionals are performed in the known regions of octupole deformed nuclei and their vicinity. This allows to estimate theoretical uncertainties in the description of physical observables. In addition, the results of our investigation are consistently compared with the ones obtained in the HFB approach with the Gogny forces and, in particular, with the MM results presented in Ref. [51]. This investigation is a continuation of our previous efforts to understand the accuracy and theoretical uncertainties (and their sources) in the description of the ground state observables [54], the extension of the nuclear landscape [54, 55, 62] and the properties of superheavy nuclei [56].

The paper is organized as follows. Section II describes the details of the solutions of the relativistic Hartree-

Bogoliubov equations. The analysis of octupole deformation in the actinides with  $Z = 86 - 106, N \sim 136$  is presented in Sec. III. Sec. IV contains the discussion of octupole deformation in the  $A \sim 146$  mass region. The impact of pairing strength on the relative energies of quadrupole and octupole minima is discussed in Sec. V. Sec. VI is devoted to the discussion of the impact of the softness of potential energy surfaces on the rotational properties of actinides. A global analysis of octupole deformation covering the full nuclear landscape for nuclei up to  $Z = 106$  is presented in Sec. VII. Finally, Sec. VIII summarizes the results of our work.

## II. THE DETAILS OF THE THEORETICAL CALCULATIONS

The calculations have been performed in the Relativistic-Hartree-Bogoliubov (RHB) approach for which a new parallel computer code RHB-OCT has been developed using as a basis the octupole deformed RMF+BCS code DOZ developed in Ref. [2]. Only axial reflection asymmetric shapes are considered in the RHB-OCT code. The parallel version allows simultaneous calculations for a significant number of nuclei and deformation points in each nucleus.

The calculations in the RHB-OCT code perform the variation of the function

$$E_{RHB} + \sum_{\lambda=2,3} C_{\lambda 0} (\langle \hat{Q}_{\lambda 0} \rangle - q_{\lambda 0})^2 \quad (1)$$

employing the method of quadratic constraints. Here  $E_{RHB}$  is the total energy (see Ref. [54] for more details of its definition) and  $\langle \hat{Q}_{\lambda 0} \rangle$  denote the expectation value of the quadrupole ( $\hat{Q}_{20}$ ) and octupole ( $\hat{Q}_{30}$ ) moments which are defined as

$$\hat{Q}_{20} = 2z^2 - x^2 - y^2, \quad (2)$$

$$\hat{Q}_{30} = z(2z^2 - 3x^2 - 3y^2). \quad (3)$$

$C_{20}$  and  $C_{30}$  in Eq. (1) are corresponding stiffness constants [63] and  $q_{20}$  and  $q_{30}$  are constrained values of the quadrupole and octupole moments. In order to provide the convergence to the exact value of the desired multipole moment we use the method suggested in Ref. [64].

Here the quantity  $q_{\lambda 0}$  is replaced by the parameter  $q_{\lambda 0}^{eff}$ , which is automatically modified during the iteration in such a way that we obtain  $\langle \hat{Q}_{\lambda 0} \rangle = q_{\lambda 0}$  for the converged solution. This method works well in our constrained calculations. We also fix the (average) center-of-mass of the nucleus at the origin with the constraint

$$\langle \hat{Q}_{10} \rangle = 0 \quad (4)$$

on the center-of-mass operator  $\hat{Q}_{10}$  in order to avoid a spurious motion of the center-of-mass.

The charge quadrupole and octupole moments are defined as

$$Q_{20} = \int d^3r \rho(\mathbf{r}) (2z^2 - r_{\perp}^2), \quad (5)$$

$$Q_{30} = \int d^3r \rho(\mathbf{r}) z(2z^2 - 3r_{\perp}^2) \quad (6)$$

with  $r_{\perp}^2 = x^2 + y^2$ . In principle these values can be directly compared with experimental data. However, it is more convenient to transform these quantities into dimensionless deformation parameters  $\beta_2$  and  $\beta_3$  using the relations

$$Q_{20} = \sqrt{\frac{16\pi}{5}} \frac{3}{4\pi} Z R_0^2 \beta_2, \quad (7)$$

$$Q_{30} = \sqrt{\frac{16\pi}{7}} \frac{3}{4\pi} Z R_0^3 \beta_3 \quad (8)$$

where  $R_0 = 1.2A^{1/3}$ . These deformation parameters are more frequently used in experimental works than quadrupole and octupole moments. In addition, the potential energy surfaces (PES) are plotted in this manuscript in the  $(\beta_2, \beta_3)$  deformation plane.

In order to avoid the uncertainties connected with the definition of the size of the pairing window [65], we use the separable form of the finite range Gogny pairing interaction introduced by Tian et al [66]. Its matrix elements in  $r$ -space have the form

$$\begin{aligned} V(\mathbf{r}_1, \mathbf{r}_2, \mathbf{r}'_1, \mathbf{r}'_2) &= \\ &= -fG\delta(\mathbf{R}-\mathbf{R}')P(r)P(r')\frac{1}{2}(1-P^\sigma) \end{aligned} \quad (9)$$

with  $\mathbf{R} = (\mathbf{r}_1 + \mathbf{r}_2)/2$  and  $\mathbf{r} = \mathbf{r}_1 - \mathbf{r}_2$  being the center of mass and relative coordinates. The form factor  $P(r)$  is of Gaussian shape

$$P(r) = \frac{1}{(4\pi a^2)^{3/2}} e^{-r^2/4a^2} \quad (10)$$

The two parameters  $G = 738 \text{ fm}^3$  and  $a = 0.636 \text{ fm}$  of this interaction are the same for protons and neutrons and have been derived in Ref. [66] by a mapping of the  $^1S_0$  pairing gap of infinite nuclear matter to that of the Gogny force D1S [67].

The scaling factor  $f$  in Eq. (9) is determined by a fine tuning of the pairing strength in a comparison between experimental moments of inertia and those obtained in cranked RHB calculations with the CEDF NL3\* (see Ref.

[54] for details). It is fixed at  $f = 1.0$  in the  $Z \geq 88$  actinides and superheavy nuclei, at  $f = 1.075$  in the  $56 \leq Z \leq 76$  and at  $f = 1.12$  in the  $Z \leq 44$  nuclei. Between these regions, i.e. for  $44 \leq Z \leq 56$  and for  $76 \leq Z \leq 88$ , the scaling factor  $f$  gradually changes with  $Z$  in a linear interpolation. The weak dependence of the scaling factor  $f$  on the CEDF has been seen in the studies of pairing and rotational properties in the actinides in Refs. [68, 69] and pairing gaps in spherical nuclei in Ref. [54]. Thus, the same scaling factor  $f$  as defined above for the CEDF NL3\* is used in the calculations with DD-PC1, DD-ME2 and DD-ME $\delta$ . Considering the global character of this study, this is a reasonable choice.

The truncation of the basis is performed in such a way that all states belonging to the major shells up to  $N_F = 16$  fermionic shells for the Dirac spinors and up to  $N_B = 20$  bosonic shells for the meson fields are taken into account (for details see Ref. [70]). Considering that the calculations are performed in the vicinity of the normal deformed minimum, this truncation of the basis provides sufficient numerical accuracy. The potential energy surfaces are calculated in constrained calculations in the  $(\beta_2, \beta_3)$  plane for the  $\beta_2$  values ranging from  $-0.2$  up to  $0.4$  and for the  $\beta_3$  values ranging from  $0.0$  up to  $0.3$  with a deformation step of  $0.02$  in each direction. The energies of the local minima are defined in unconstrained calculations.

The effect of octupole deformation can be quantitatively characterized by the quantity  $\Delta E_{oct}$  defined as

$$\Delta E_{oct} = E^{oct}(\beta_2, \beta_3) - E^{quad}(\beta'_2, \beta'_3 = 0) \quad (11)$$

where  $E^{oct}(\beta_2, \beta_3)$  and  $E^{quad}(\beta'_2, \beta'_3 = 0)$  are the binding energies of the nucleus in two local minima of potential energy surface; the first minimum corresponds to octupole deformed shapes and second one to the shapes with no octupole deformation. The quantity  $|\Delta E_{oct}|$  represents the gain of binding due to octupole deformation. It is also an indicator of the stability of the octupole deformed shapes. Large  $|\Delta E_{oct}|$  values are typical for well pronounced octupole minima in the PES; for such systems the stabilization of static octupole deformation is likely. On the contrary, small  $|\Delta E_{oct}|$  values are characteristic for soft (in octupole direction) PES typical for octupole vibrations. In such systems beyond mean field effects can play an important role. They have profound effect on the spectroscopy of the nuclei, in particular, on the E1 and enhanced E3 transition strengths [17, 71, 72], and on the energy splittings of the positive and negative parity branches of alternating parity rotational bands [17, 73]. On the other hand, octupole beyond mean field correlations do not affect in a significant way the trends and systematics of binding energies [74].

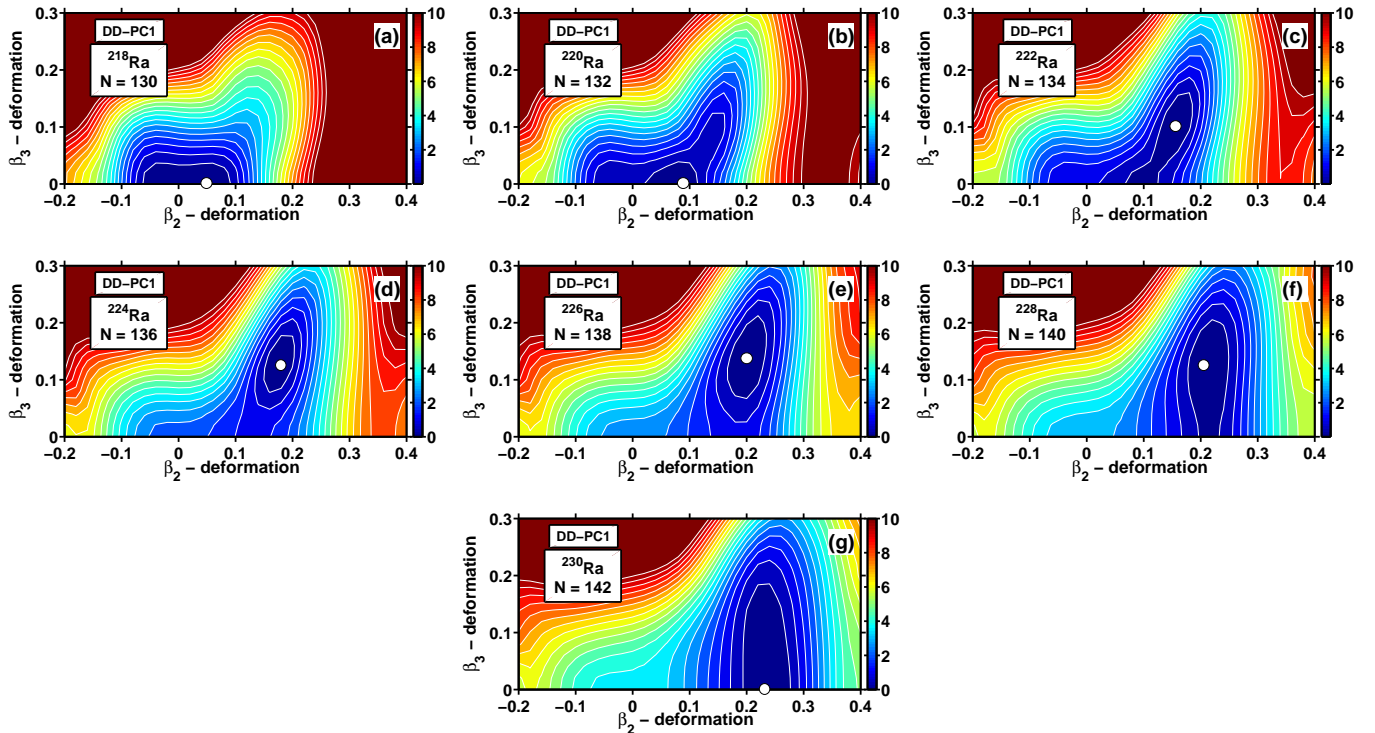


FIG. 2. (Color online) The same as Fig. 1, but for the Ra isotopes.

### III. OCTUPOLE DEFORMATION IN ACTINIDES

Several studies of the octupole deformation in the ground states of actinides and its impact on spectroscopic properties of these nuclei have been performed so far in the CDFT framework. The first relativistic study of octupole shapes in the ground states of atomic nuclei has been performed twenty years ago in Ref. [47]; in this manuscript radium isotopes have been investigated in the RMF+BCS approach using monopole pairing with constant pairing gap and the CEDFs NL1, NL-SH and PL-40. Shape evolution from spherical to octupole-deformed shapes has been studied in even-even Th isotopes in the RMF+BCS framework in Ref. [5] using monopole pairing with constant pairing gap and the NL3\* and PK1 functionals. Octupole deformed shapes in  $^{226}\text{Ra}$  have been investigated earlier in Ref. [48] within the same approach but with NL1 and NL3 functionals. The potential energy surfaces and octupole deformations of the ground states of even-even  $^{222}\text{--}^{232}\text{Th}$  and  $^{218}\text{--}^{228}\text{Ra}$  nuclei have been studied in the RHB framework with the DD-PC1 functional and separable pairing forces in Refs. [12, 13]. The mapping of these potential energy surfaces onto an equivalent Hamiltonian of the *sdf* interacting boson model (IBM) allowed to determine its parameters. Then, the resulting IBM Hamiltonian was used to calculate excitation spectra and transition rates for positive- and negative-parity states in these nuclei [12, 13]. Recently, first gen-

erator coordinate method studies taking into account dynamical correlations and quadrupole-octupole shape fluctuations have been undertaken in  $^{224}\text{Ra}$  employing the PC-PK1 functional [17]. They reveal rotation-induced octupole shape stabilization.

It is clear that these studies were quite limited in scope and the selection of nuclei was guided by the previous studies in non-relativistic frameworks. A global review of octupole deformed nuclei in this mass region paints a much richer picture. Our RHB calculations indicate that not only Ra and Th nuclei (as suggested by previous studies) can have either stable octupole deformation or be octupole soft, but also U, Pu, Cm, Cf, Fm, No and Sg nuclei possess these properties. The potential energy surfaces obtained in the RHB calculations with the DD-PC1 functional are shown in Figs. 1, 2, 4, 5, 6, 8, 9, and 10 below for the nuclei in the Rn, Ra, Th, U, Pu, Cm, Cf and Fm isotope chains. According to previous global surveys of the performance of the state-of-the-art CEDFs presented in Refs. [54, 56], this is one of the best CEDFs. Neutron number dependencies of calculated equilibrium quadrupole and octupole deformations as well as the gains in binding due to octupole deformation for these isotope chains are presented for five CEDFs in Figs. 3, 7 and 11 below. For simplicity of the discussion of the results and their comparison with available experimental data and other theoretical approaches, they are discussed on the “chain-by-chain” basis in the next subsections.

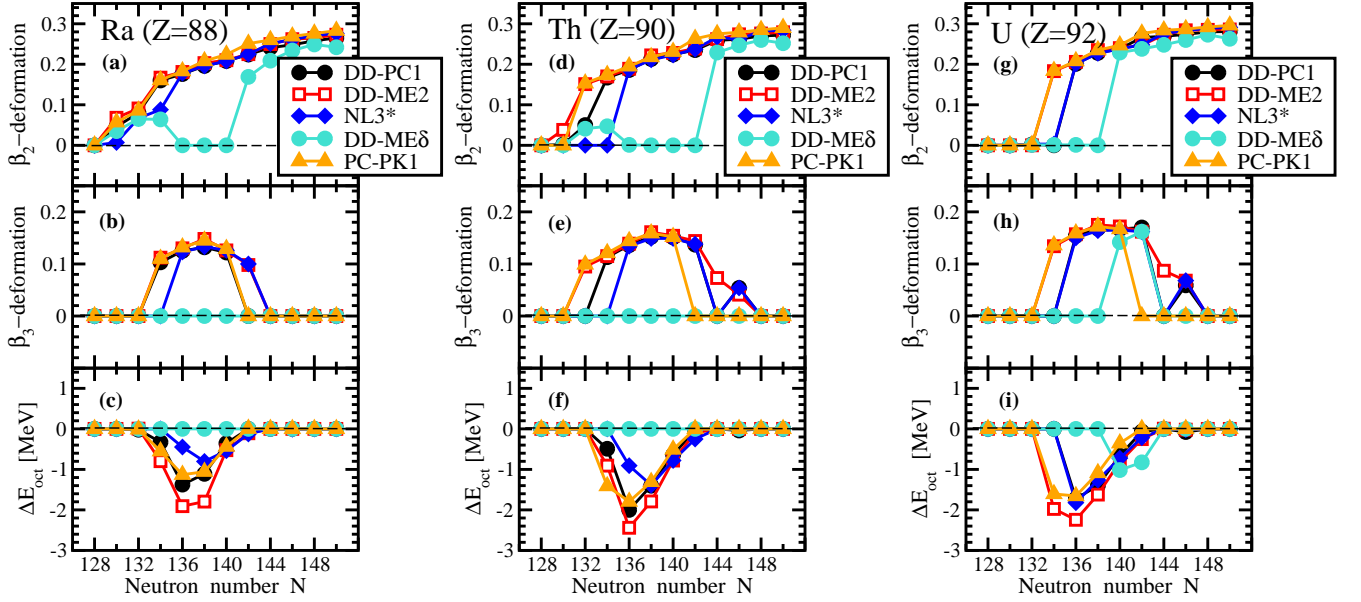


FIG. 3. (Color online) The calculated equilibrium quadrupole  $\beta_2$  (panels (a), (d) and (g)) and octupole  $\beta_3$  (panels (b), (e) and (h)) deformations as well as the  $\Delta E^{oct}$  quantities (panels (c), (f) and (i)). The results of the RHB calculations with five indicated functionals are presented for the Ra, Th and U isotope chains.

## A. Discussion: theory versus experiment

### 1. Rn isotopes

No octupole deformation is predicted in the Rn isotopes of interest (see Table I). The potential energy surfaces are soft in octupole direction for the  $N = 136, 138$   $^{222,224}\text{Rn}$  nuclei (Fig. 1). This is in agreement with the analysis of experimental data presented in Refs. [20, 75] which strongly suggests that the  $^{218-222}\text{Rn}$  isotopes behave like octupole vibrators, thus supporting the presence of a considerable octupole softness of the potential energy surfaces.

The MM calculations of Ref. [76] with a Woods Saxon potential suggest that only the  $^{222-224}\text{Rn}$  isotopes with  $N = 136-138$  have non-zero octupole deformation. However, the gain in binding due to octupole deformation is rather small ( $\sim 100$  keV). A wider range of octupole deformed Rn isotopes with  $N = 132-140$  (with a maximum value of  $|\Delta E^{oct}| = 0.85$  MeV at  $N = 134$ ) and  $N = 146$  is predicted in Ref. [51] in MM calculations with a folded Yukawa potential (see Table I). Ref. [77] shows that at least  $^{220}\text{Rn}$  has non-zero octupole deformation in the ground state in the HFB calculations with the D1S and D1M Gogny forces. However, this is octupole soft nucleus with a relative small gain in binding due to octupole deformation ( $|\Delta E^{oct}| < 0.25$  MeV).

### 2. Ra isotopes

Potential energy surfaces of the Ra isotopes are shown in Fig. 2. Weakly deformed minima with  $\beta_3 = 0.0$

are the lowest in energy in the  $^{218,220}\text{Ra}$  nuclei with  $N = 130, 132$ . The increase of neutron number leads to the formation of an octupole minimum which becomes pronounced at  $N = 136, 138$ . At higher neutron numbers the potential energy surfaces become soft in octupole direction.

The maximum gain in binding energy due to octupole deformation  $|\Delta E^{oct}|$  takes place at  $N \sim 136$  for the CEDFs PC-PK1, DD-ME2 and DD-PC1 and at  $N = 138$  for NL3\* (Fig. 3). For these functionals the maximum  $|\Delta E^{oct}|$  values vary from around 1 MeV for NL3\* and PC-PK1 up to 2 MeV for DD-ME2. The DD-ME $\delta$  functional does not predict octupole deformation for the nuclei of interest which contradicts both to experimental data (see Ref. [1]) and the predictions of other models (see below).

Experimental data suggest that in the Ra isotopes the maximum effect of octupole deformation is seen at  $N \sim 136$  [1]. For example, the  $N = 136$  isotope has the lowest energy of the  $1^-$  bandhead of the negative parity band. There are some differences in the predictions of the various models for the range of nuclei with octupole deformation and for the neutron numbers at which the maximum gain in binding due to octupole deformation takes place. For example, the MM calculations based on folded Yukawa [51] (see also Table I) and Woods-Saxon potentials [76] predict octupole deformation in the  $N = 130-138$  and  $N = 134-138$  isotopes, respectively. In these models, the maximum gain in binding due to octupole deformation takes place at  $N = 132$  and  $N = 136$ , respectively. Note that the results obtained with a Woods-Saxon potential are closer to experimental data [1]. The HFB calculations with the D1S



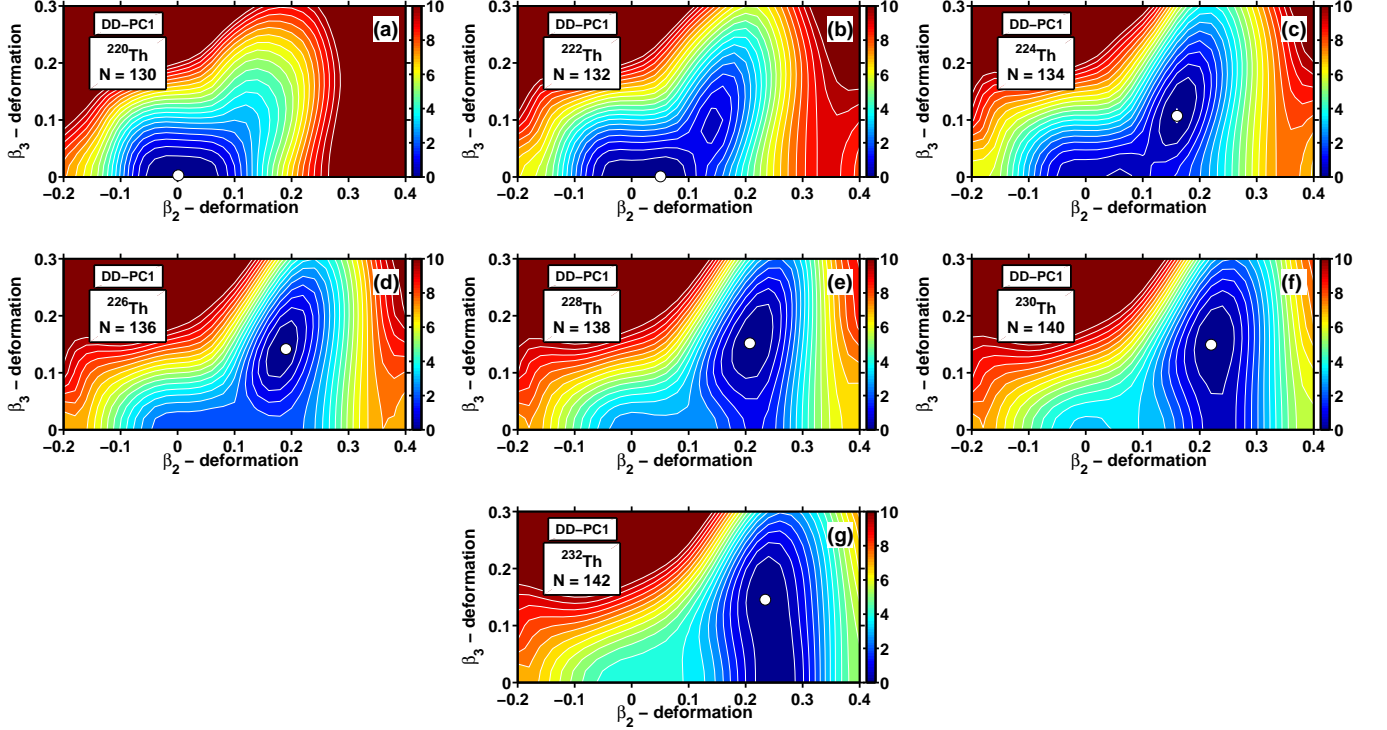


FIG. 4. (Color online) The same as Fig. 1, but for the Th isotopes.

Gogny force [78] and the Barcelona-Catania-Paris (BCP) energy density functional [79] show that there exists non-vanishing octupole deformation for the Ra isotopes with  $N = 130 - 140$  and with  $N = 130 - 142$ , respectively. In both cases the maximum gain in binding energy due to octupole deformation takes place at  $N = 134$ .

### 3. Th isotopes

The evolution of the topology of the PESs of the Th isotopes is presented in Fig. 4 as a function of neutron number. It is similar to the one discussed above for the Ra isotopes. Well pronounced octupole minima exist in the  $N = 136$  and  $138$  Th isotopes.

The calculations with the DD-PC1 and DD-ME2 functionals suggest that in whole region under study the Th isotopes are characterized by the strongest octupole deformation effects (see Fig. 3). However, this is not the case for PC-PK1, where the octupole deformation effects are comparable in the Th and U nuclei, and for NL3\*, where they are more pronounced in the U isotopes. In the Th isotopes the maximum of  $|\Delta E^{oct}|$  is located at  $N = 136$  for DD-PC1, DD-ME2, and PC-PK1 and at  $N = 138$  for NL3\* (Fig. 3). The predictions of the DD-ME $\delta$  functional disagree with all other model calculations and experimental data.

Experimental data suggest that the maximal effects of octupole deformation in the Th isotopes are seen at

$N \sim 136$  [1]. For example, the  $N = 136$  isotope has the lowest energy of the  $1^-$  bandhead of the negative parity band. The MM calculations based on folded Yukawa [51] and Woods-Saxon [76] potentials predict octupole deformation in the  $N = 130 - 138$  (see Table I) and  $N = 132 - 138$  (see Ref. [76]) isotopes, respectively. In these models, the maximum gain in binding due to octupole deformation takes place at  $N = 132$  and  $N = 134$ , respectively. The results obtained with Woods-Saxon potential are closer to experimental data [1]. The HF+BCS calculations with the Gogny D1S force [78] predict octupole deformation in the ground states of the  $^{222-228}\text{Th}$  nuclei with  $N = 132 - 138$ ; the maximum gain in binding due to octupole deformation is located at  $N = 132, 134$ .

### 4. U isotopes

The PESs of the U isotopes calculated with DD-PC1 are shown in Fig. 5 and Fig. 17 below. The spherical minimum is the lowest in energy for the isotope  $^{224}\text{U}$  with  $N = 132$ . The coexistence of spherical and octupole deformed minima is clearly seen in the  $N = 134$  and  $N = 136$  isotopes. However, at higher neutron number the potential energy landscape is dominated by an octupole deformed minimum which becomes extremely soft above  $N = 140$ . At and above  $N = 148$  octupole deformation vanishes and only a quadrupole deformed minimum is present (see Fig. 17 below).

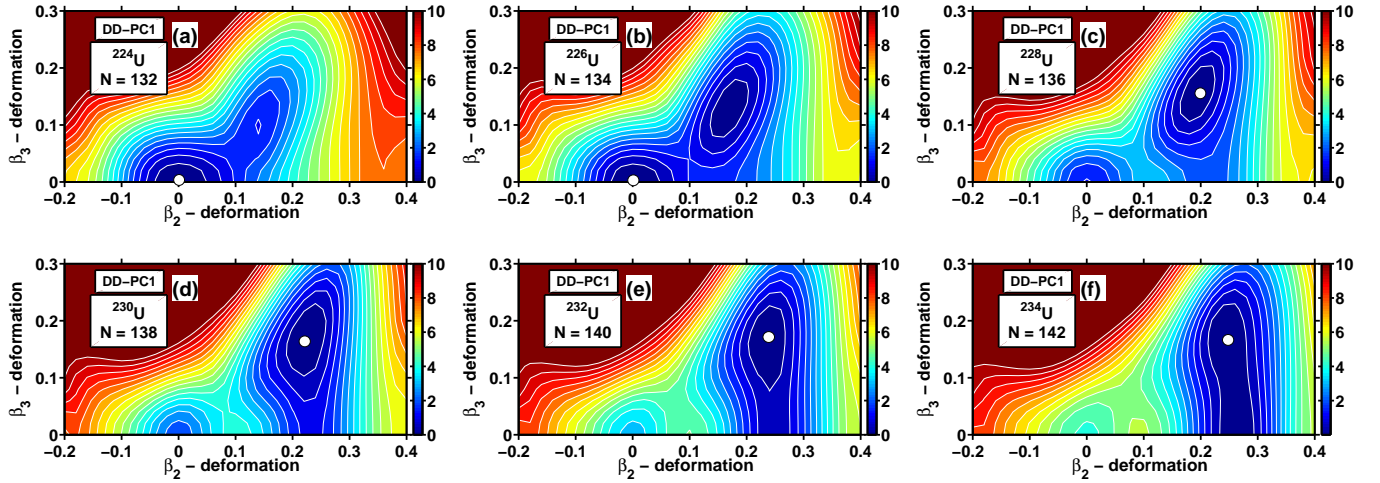


FIG. 5. (Color online) The same as Fig. 1, but for the U isotopes.

The maximum gain in binding energy due to octupole deformation takes place at  $N \sim 136$  with  $|\Delta E^{oct}| \geq 1.0$  MeV for  $N = 134, 136$  and  $138$  for DD-ME2 and PC-PK1 and for  $N = 136$  and  $138$  for NL3\* and DD-PC1 (Fig. 3). Again, the results for DD-ME $\delta$  are in contradiction with all other functionals and with experiment. An alternative parity rotational band, indicative of static octupole deformation, is observed in the nucleus  $^{226}\text{U}$  with  $N = 134$  in Ref. [80]. The experimental data on  $^{228}\text{U}$  is restricted to the ground and  $2^+$  states [81]; so no decision about the presence of static octupole deformation is possible in this nucleus. Octupole vibrational bands with  $1^-$  bandheads, located at extremely low excitation energies of 366.65 keV and 562.19 keV, are observed in  $^{230}\text{U}$  and  $^{232}\text{U}$ , respectively [81]. They are indicative of extreme octupole softness of the potential energy surfaces.

The MM calculations based on different phenomenological potentials and on different liquid drop formulas predict octupole deformed U nuclei at  $N = 128 - 134$  (see Fig. 2 in Ref. [9]). In these calculations the maximum gain in binding due to octupole deformation takes place at lower  $N$  as compared with CDFT. For example, it is located at  $N = 132$  (Table I) in the MM calculations of Ref. [51]. The HFB calculations with several versions of the Gogny force show that the U isotopes with  $N = 130 - 138$  have non-zero octupole deformation [10].

### 5. Pu isotopes

The PESs of the Pu isotopes calculated with DD-PC1 are shown in Fig. 6 and Fig. 18 below. The spherical minimum is the lowest in energy for the isotope  $^{224}\text{Pu}$  with  $N = 130$ . The coexistence of a spherical (which is the lowest in energy) and an octupole deformed minima is clearly seen in the  $N = 132$  isotope. A well pronounced octupole deformed minimum exists in the  $N = 134$  and  $136$  isotopes. However, at higher neutron number the

PESs become extremely soft in octupole deformation so that the position of the minimum (finite octupole deformation at  $N = 140$  and  $146$  or vanishing octupole deformation at  $N = 142, 144$  and  $148$ ) depends on fine details of the underlying single-particle structure. Note that the energy gain due to octupole deformation is very small for  $N = 146$ , namely, less than 100 keV (Table I). The maximum gain in binding energy due to octupole deformation is found at  $N = 134$  for PC-PK1 and DD-ME2 and at  $N = 136$  for NL3\* and DD-PC1 (Fig. 7). Only in these isotopes the gain due to octupole deformation  $|\Delta E^{oct}|$  is close to or exceeds 1.0 MeV. The results for DD-ME $\delta$  are again in contradiction with all other functionals.

The predictions of CDFT differ from those of the non-relativistic models. The HFB calculations with Gogny forces of Ref. [10] indicate that the isotopes  $^{224}-^{232}\text{Pu}$  with  $N = 130 - 138$  have finite octupole deformations in the ground states; the maximum gain in binding due to octupole deformation takes place at  $N = 132$ . The MM calculations of Ref. [51] predict octupole deformation only for the isotopes  $^{222}-^{228}\text{Pu}$  ( $N = 128 - 134$ ) with a maximum gain in binding due to octupole deformation at  $N = 130$  (see Table I).

At present, it is impossible to discriminate between the predictions of these models because of the limitations of experimental data. Only the  $0^+$  ground state has been observed in the nuclei  $^{228}-^{234}\text{Pu}$  with  $N = 134 - 140$  (which does not allow to define the presence or absence of octupole deformation) and no experimental data are available for lighter Pu isotopes [81]. On the other hand, octupole vibrational bands have been observed [81] in the isotopes  $^{236}-^{230}\text{Pu}$  ( $N = 142 - 146$ ) with bandheads located at low excitation energies of 698, 605 and 597 keV, respectively. This suggests a substantial octupole softness of the potential energy surfaces of these nuclei. Indeed, there are some indications of the stabilization of octupole deformation at high spin in  $^{240}\text{Pu}$  [82, 83] (see also Sec. VI).

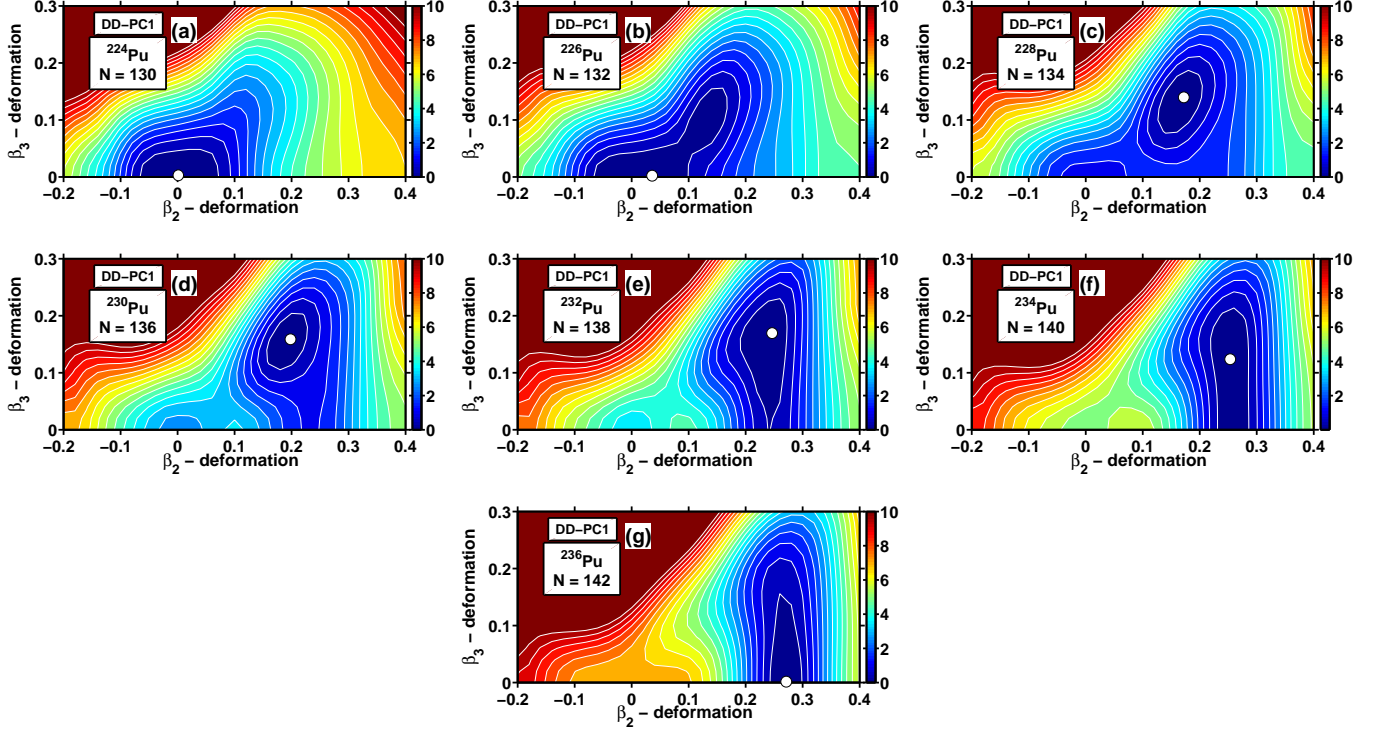


FIG. 6. (Color online) The same as Fig. 1, but for the Pu isotopes.

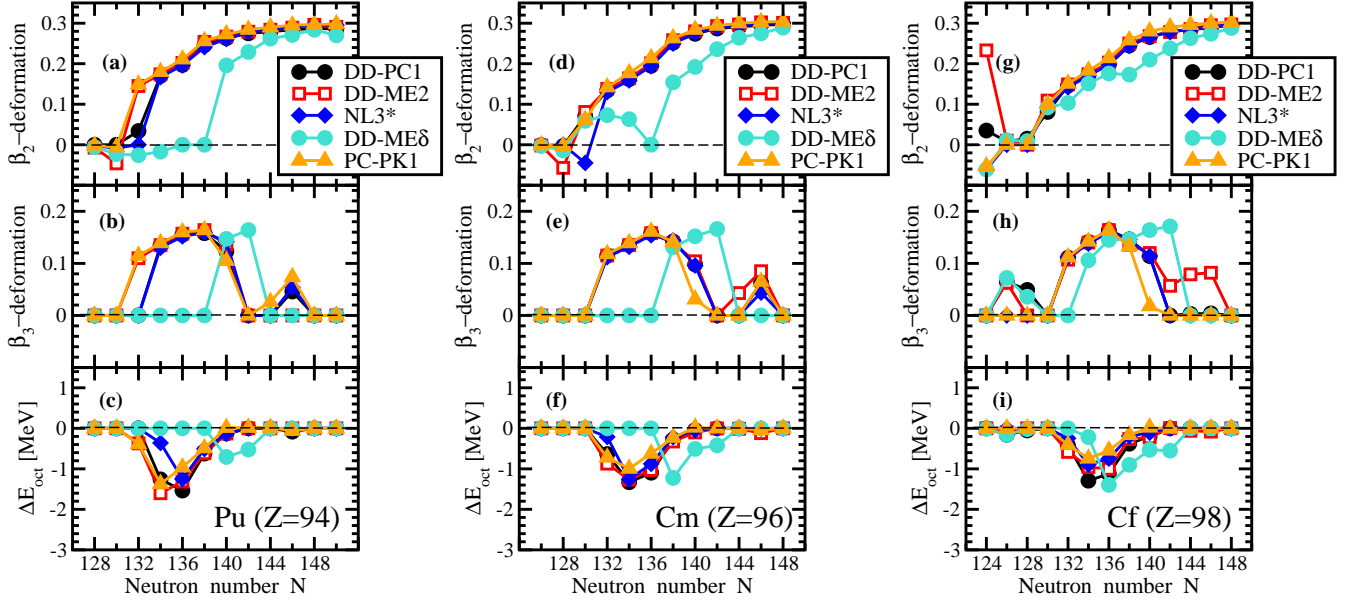


FIG. 7. (Color online) The same as Fig. 3, but for the Pu, Cm and Cf isotopes.

#### 6. Cm isotopes.

PESs of Cm isotopes are presented in Fig. 8. Spherical and weakly deformed minima are seen in the isotopes  $^{224,226}\text{Cm}$  with  $N = 128 - 130$ . The increase of neutron number leads to the development of an octupole deformed minimum which becomes especially pronounced

in the nuclei  $^{230,232}\text{Cm}$  with  $N = 134, 136$ . With a further increase of neutron number the potential energy surfaces become extremely soft in octupole direction. The maximum of the gain in binding energy due to octupole deformation ( $|\Delta E^{oct}| \sim 1.0$  MeV) takes place at  $N \sim 134$  for the NL3\*, PC-PK1, DD-ME2 and DD-PC1 CEDFs (Fig. 7). The results for DD-ME $\delta$  are in contradiction



with all other functionals.

The HFB calculations with Gogny forces of Ref. [10] indicate that the isotopes  $^{226-230}\text{Cm}$  with  $N = 130 - 134$  have non-zero octupole deformation in the ground states; the maximum gain in binding due to octupole deformation of around several hundred keV takes place at  $N = 130$ . The MM calculations of Ref. [51] predict octupole deformation only for the isotopes  $^{224-228}\text{Cm}$  ( $N = 128 - 132$ ) with a maximum gain in binding due to octupole deformation ( $|\Delta E^{oct}| \sim 0.8$  MeV) at  $N = 130$  (see Table I). Since experimental data do not exist for the Cm isotopes with  $N \leq 136$  and only ground states are observed in the nuclei  $^{234,236}\text{Cm}$  with  $N = 138, 140$  [81], there is no way to discriminate between the predictions of the models.

### 7. Cf isotopes

The PESs of the Cf isotopes are displayed in Fig. 9. An unusual feature of the  $^{224,226}\text{Cf}$  isotopes with  $N = 126, 128$  is the presence of the minimum in the PES with almost zero quadrupole deformation and octupole deformation  $\beta_3 \sim 0.1$ . However, the PESs are soft in octupole direction in  $^{224}\text{Cf}$  and both in quadrupole and octupole directions in  $^{226}\text{Cf}$ . An octupole deformed minimum starts to develop in  $N = 132$   $^{230}\text{Cf}$  and becomes especially pronounced in  $^{232,234}\text{Cf}$ . A further increase of neutron number leads to PES which are extremely soft in octupole direction. The maximum of the gain in binding energy due to octupole deformation ( $|\Delta E^{oct}| \sim 1.0$  MeV) takes place either at  $N = 134$  or at  $N = 136$  for NL3\*, PC-PK1, DD-ME2 and DD-PC1 (Fig. 7). The results for DD-ME $\delta$  are in contradiction with all other functionals.

The HFB calculations with Gogny forces of Ref. [10] indicate that isotopes  $^{228-232}\text{Cf}$  with  $N = 130 - 134$  have non-zero octupole deformation in the ground states. Dependent on the functional the maximum gain in binding due to octupole deformation of around 0.5 MeV takes place either at  $N = 130$  or at  $N = 132$ . The MM calculations of Ref. [51] predict octupole deformation only for the isotopes  $^{224-228}\text{Cf}$  ( $N = 126 - 130$ ) with a maximum gain in binding due to octupole deformation ( $|\Delta E^{oct}| \sim 0.6$  MeV) at  $N = 128$  (Table I). Since experimental data do not exist for the Cf isotopes with  $N \leq 138$  and only the ground state is observed in the  $N = 140$   $^{238}\text{Cf}$  nucleus [81], there is no way to discriminate between the predictions of the models.

### 8. Fm isotopes

For a given neutron number, the PESs of the Fm isotopes are very similar to the ones of the Cf isotopes (compare Figs. 10 and 9). Thus, the discussion of the evolution of PESs as a function of the neutron number presented in Sec. III A 8 is also applicable to the Fm isotopes. The results of the calculations with NL3\*, PC-PK1, DD-

ME2 and DD-PC1 show a similar evolution of  $\Delta E^{oct}$  as a function of neutron number (Fig. 11). The maximum in  $|\Delta E^{oct}|$  is seen either at  $N = 134$  (DD-PC1 and PC-PK1) or at  $N = 136$  (NL3\* and DD-ME2); its value is located in the 0.5 – 1.0 MeV range. The results for DD-ME $\delta$  differ substantially from all other functionals.

The MM approach predicts octupole deformation only in the  $N = 126, 128$  nuclei (Table I) with rather modest gains in binding due to octupole deformation. The maximum of  $|\Delta E^{oct}|$  is located at  $N = 128$ . The HFB calculations with Gogny forces show the presence of octupole deformation in the isotopes  $^{230-232}\text{Fm}$  with  $N = 130 - 132$  [10]. No experimental data are available for the Fm isotopes with  $N \leq 140$  [81]. Thus, the predictions of different models cannot be discriminated.

### 9. No, Rf and Sg isotopes

Our RHB calculations predict octupole deformed No, Rf and Sg isotopes (see Table I). However, most of these nuclei are octupole soft with marginal gains in binding due to octupole deformation. In addition, there is a substantial difference between the NL3\* and DD-PC1 functionals. For example, only the  $N = 136$   $^{238}\text{No}$  nucleus is predicted to be octupole deformed in the calculations with DD-PC1. On the contrary, the  $N = 134 - 140$   $^{236-242}\text{No}$  nuclei are octupole deformed in NL3\*. No octupole deformed Rf nuclei are predicted in DD-PC1, while the  $N = 138 - 142$   $^{242-246}\text{Rf}$  nuclei have nonzero octupole deformation in the ground states (Table I). Note that the No, Rf and Sg nuclei with nonzero octupole deformation are located at or near the two-proton drip line (see Fig. 19 below) so their experimental observation could be very difficult. At present, no experimental data are available for these proton-rich nuclei [81].

The MM calculations of Ref. [51] do not predict octupole deformation for the No, Rf and Sg isotopes. The HFB calculations with Gogny forces of Ref. [10] predict nonzero  $\beta_3$  values only in the  $^{232-234}\text{No}$  nuclei.

## B. General observations

The analysis of the results of the RHB calculations and the comparison between different models reveal the following general features:

- The results of the calculations are rather similar for the CEDFs DD-ME2, DD-PC1 and PC-PK1 (see Figs. 3, 7 and 11). The results with NL3\* only slightly deviate from the ones for these functionals. Not only quadrupole and octupole equilibrium deformations as well as the gains in binding due to octupole deformation displayed in Figs. 3, 7 and 11 show these features, but also the topologies of the PESs, which affect the results of beyond mean field calculations, are similar in these four functionals

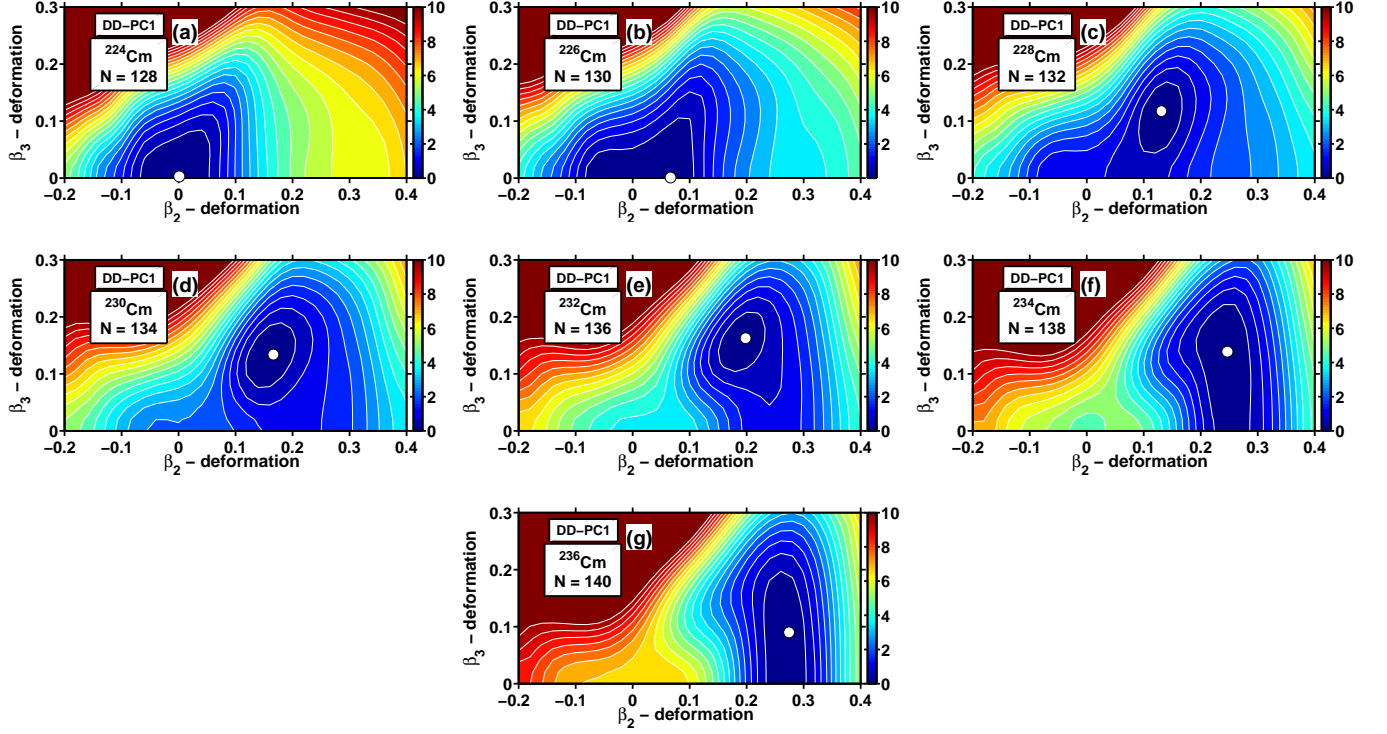


FIG. 8. (Color online) The same as Fig. 1, but for the Cm isotopes.

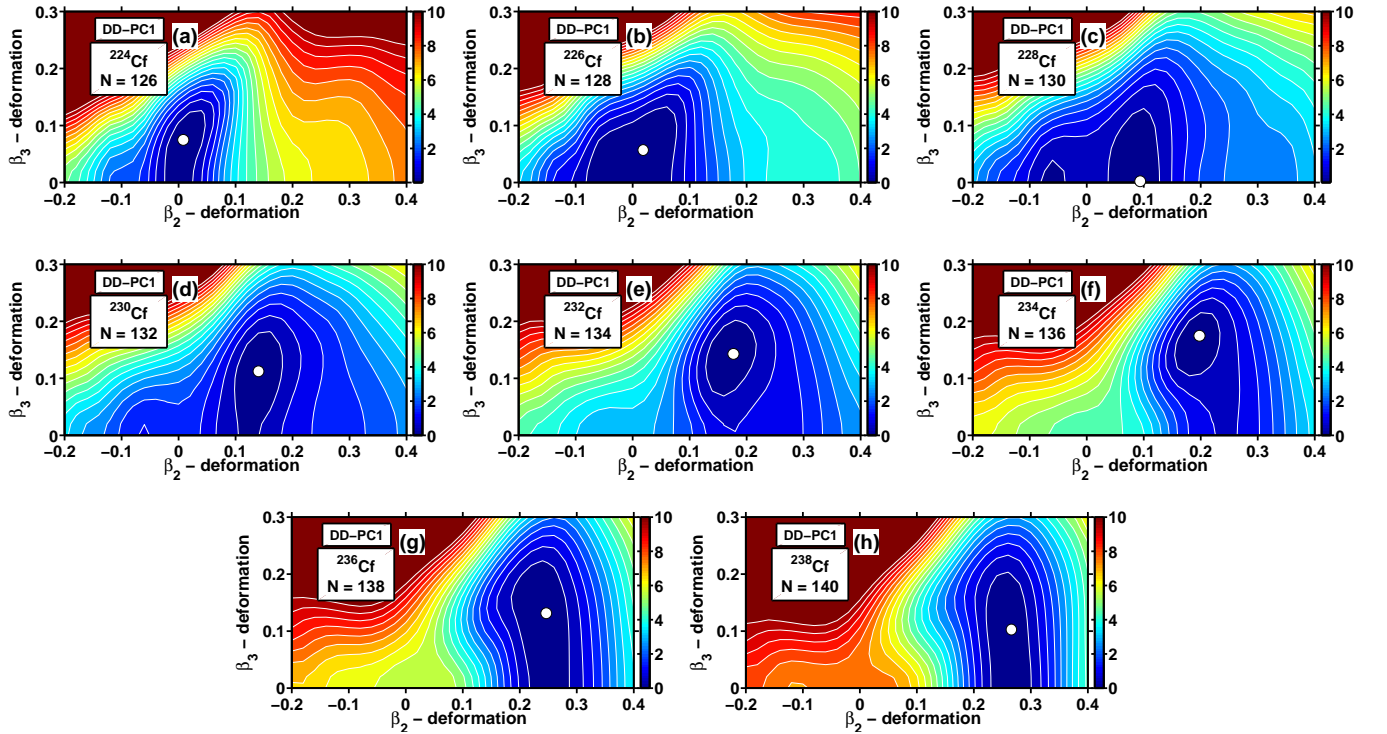


FIG. 9. (Color online) The same as Fig. 1, but for the Cf isotopes.

(see Fig. 12). The predictions obtained with the CEDF DD-ME $\delta$  contradict to all available model calculations and to experimental data. Therefore, the results obtained with this functional will not be discussed in this subsection.

- In the RHB calculations with DD-ME2, DD-PC1, NL3\* and PC-PK1 a gradual increase of quadrupole deformation is typically seen in the  $N = 130 - 140$  range (see Figs. 3, 7 and 11). At higher  $N$  value, the  $\beta_2$  deformation is nearly constant.
- The center of the island of octupole deformation, defined in terms of maximum gain in binding due to octupole deformation, is located at  $Z = 90 - 92$  and  $N = 136$  in the RHB calculations with the CEDFs DD-PC1, DD-ME2 and PC-PK1. This agrees with the experiment [1] and with the results obtained within the HFB framework based on Gogny forces [10] and the MM calculations based on Woods-Saxon potentials [76]. The MM calculations of Ref. [51] with folded Yukawa potentials favor somewhat lower neutron numbers  $N = 132 - 134$ . In these calculations the neutron number  $N$  of the nucleus with maximum gain in binding due to octupole deformation in a given isotope chain decreases with increasing proton number  $Z$  down to  $N = 128$  in the Cf and Fm isotopes. A similar but less pronounced trend is seen in the HFB calculations with the Gogny forces. On the contrary, for relativistic functionals this decrease is only 2 neutrons in going from the Th and U isotopes to the Cf and Fm isotopes (see Figs. 3, 7 and 11). Thus, the CDFT predictions favor the experimental observation of these octupole deformed nuclei as compared with non-relativistic models since the island of octupole deformed nuclei is located closer to the beta-stability line in the RHB calculations. In particular, octupole deformed Pu, Cm, and Cf nuclei could be within the reach of future dedicated experiments.

#### IV. OCTUPOLE DEFORMATION IN THE BA-CE-ND-SM REGION

Octupole deformation is predicted also in the ground states of the Ba, Ce, Nd and Sm isotopes. The results for equilibrium quadrupole and octupole deformations and the gains in binding due to octupole deformation are summarized in Fig. 13.

Several features are typical for this mass region. First, the gain in binding due to octupole deformation is substantially smaller ( $|\Delta E^{oct}|$  is typically around 0.5 MeV) than in the actinides. Thus, the stabilization of octupole deformation at the ground state is less likely in this region as compared with actinides.

Second, the results obtained with DD-ME $\delta$  still differ from the ones obtained with other functionals. However, the differences are less pronounced as compared with the actinides where the RHB results obtained with this functional contradict drastically to experimental data and the results of other functionals. One can also see in Fig. 14 that the topologies of the PESs obtained with the five employed functionals are similar; the only difference is the fact that octupole minimum is somewhat deeper in the DD-ME2 and DD-PC1 CEDFs as compared with other functionals. Note that we will not discuss the details of the results obtained with CEDF DD-ME $\delta$  in the following.

In this mass region we focus on the presentation of the RHB results and their comparison with non-relativistic ones. In general, the island of octupole deformation predicted in the RHB calculations is close to the ones obtained in non-relativistic calculations. Moreover, it is close to the one extracted from experimental data indicating either octupole deformation or enhanced octupole correlations (see Ref. [1] for details). However, a detailed interpretation of experimental data in this mass region at the mean field level is complicated by the fact that PES are extremely soft in the octupole direction which favors the fluctuations and vibrations in this degree of freedom. For example, expected parity doublets in odd-mass nuclei, which are clear fingerprints of static octupole deformation [1], are frequently not observed even near the center of the island of octupole deformation in the lanthanides [18, 19, 26].

##### A. Xe isotopes.

Our RHB calculations (including those with the CEDFs DD-ME2, PC-PK1 and DD-ME $\delta$ , not shown in Table I) do not predict non-zero octupole deformation in the  $N \sim 88$  nuclei (Table I). On the contrary, the minimum in the PESs of the nuclei  $^{142,144}\text{Xe}$  with  $N = 86, 88$  is characterized by  $\beta_3 \sim 0.06$  in the MM calculations of Ref. [51] with a folded Yukawa potential. A non-zero  $\beta_3$  deformation is also seen in the nucleus  $^{144}\text{Xe}$   $N = 90$  in the MM calculations with a Woods-Saxon potential [84]. The HF+BCS calculations with the D1S Gogny force predict non-zero octupole deformation in  $^{142,144}\text{Xe}$  [85]. Experimental data on  $^{142,144}\text{Xe}$  [81] do not suggest the stabilization of octupole deformation at the ground state.

##### B. Ba isotopes.

A non-zero octupole deformation is predicted for the  $N = 88 - 94$   $^{144-150}\text{Ba}$  isotopes in calculations with DD-

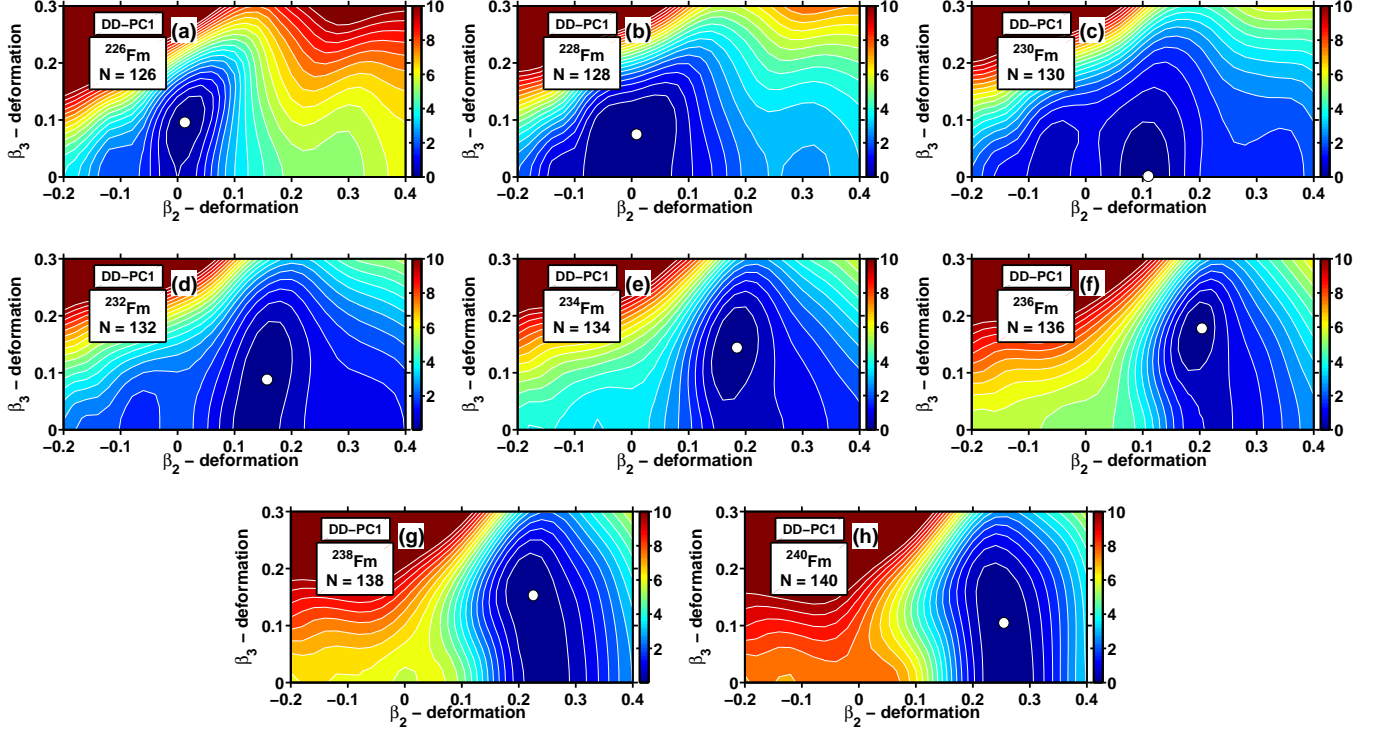


FIG. 10. (Color online) The same as Fig. 1, but for the Fm isotopes.

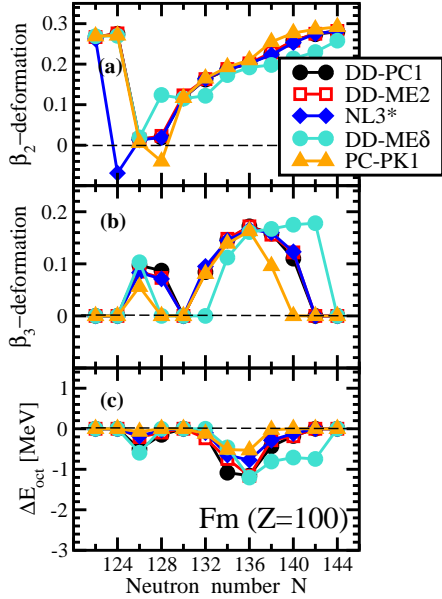


FIG. 11. (Color online) The same as Fig. 3, but for the Fm isotopes.

PC1<sup>1</sup>, for the  $N = 88 - 96$   $^{144-152}\text{Ba}$  isotopes with DD-ME2 and NL3\*, and for the  $N = 90 - 92$   $^{146-148}\text{Ba}$

<sup>1</sup> The same nuclei were predicted to have non-zero octupole deformation in the RHB calculations with DD-PC1 in Ref. [13].

isotopes with PC-PK1 (Fig. 13). The maximum gain in binding due to octupole deformation takes place at  $N = 90$  for DD-PC1 and PC-PK1, at  $N = 92$  for NL3\* and at  $N = 94$  for DD-ME2. The RMF+BCS calculations with PK1 CEDF of Ref. [49] predict a finite octupole deformation in the  $N = 88 - 98$  Ba isotopes with a maximum octupole deformation around  $N = 92 - 94$ . On the contrary, in the MM calculations with a folded Yukawa potential (Ref. [51] and Table I) only the  $N = 86 - 90$  isotopes possess non-zero octupole deformation. The MM results of Ref. [84] based on a Woods-Saxon potential show non-zero octupole deformation only in the  $N = 88 - 90$  nuclei. The HF+BCS calculations with Gogny D1S force of Ref. [86] predict non-zero octupole deformation in the  $N = 88 - 92$   $^{142-148}\text{Ba}$  nuclei with a maximum gain of binding due to octupole deformation at the nucleus  $^{144}\text{Ba}$  with  $N = 90$ .

### C. Ce isotopes.

The  $N = 88 - 92$   $^{146-150}\text{Ce}$  nuclei have  $\beta_3 \neq 0$  in the RHB calculations with the CEDFs DD-PC1, NL3\* and PC-PK1. The DD-ME2 functional provides one extra nucleus ( $N = 94$   $^{152}\text{Ce}$ ) with non-zero octupole deformation. In all functionals, the maximum of  $|\Delta E^{oct}|$  is reached at  $N = 90$ . The MM calculations with folded Yukawa [51] (see also Table I) and Woods-Saxon [84] potentials predict non-zero octupole deformation in the

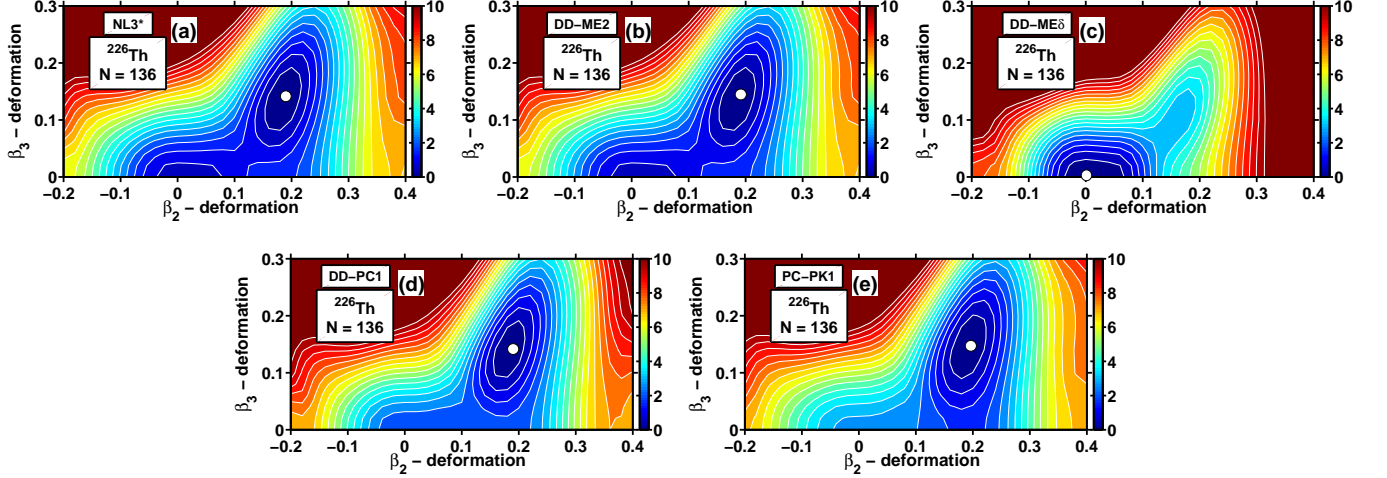


FIG. 12. (Color online) The same as Fig. 1, but for the  $^{226}\text{Th}$  obtained with indicated CEDFs

$N = 86 - 90$   $^{144-148}\text{Ce}$  and  $N = 86 - 88$   $^{144,146}\text{Ce}$  nuclei, respectively. The HF+BCS calculations with the Gogny D1S force of Ref. [86] predict octupole deformation in the  $N = 84 - 90$   $^{142-148}\text{Ce}$  nuclei.

#### D. Nd isotopes.

The  $N = 88 - 90$   $^{148-150}\text{Nd}$  nuclei are predicted to be octupole deformed with four CEDFs. The maximum gain in binding due to octupole deformation is reached at  $N = 88$  for DD-PC1 and DD-ME2 and at  $N = 90$  for NL3\* and PC-PK1. The  $N = 86 - 88$   $^{146,148}\text{Nd}$  nuclei are predicted to be octupole deformed in the MM calculations with a folded Yukawa potential (see Table I). On the contrary, the MM calculations with a Woods-Saxon potential do not predict octupole deformed Nd nuclei [84]. The  $N = 86 - 88$   $^{146-148}\text{Nd}$  isotopes are predicted to be octupole deformed in the HF+BCS calculations with the Gogny force D1S [86].

#### E. Sm isotopes.

Our calculations predict that only in the nucleus  $^{150}\text{Sm}$  a very shallow octupole minimum (with  $|\Delta E^{oct}| = 0.25$  MeV for DD-PC1 and  $|\Delta E^{oct}| = 0.09$  MeV for NL3\*) is formed. On the contrary, the RMF+BCS calculations with PK1 presented in Ref. [50] predict non-zero octupole deformation in the nuclei  $^{146-152}\text{Sm}$ . The maximum gain in binding due to octupole deformation ( $|\Delta E^{oct}| = 1.36$  MeV) takes place in the  $N = 88$   $^{150}\text{Sm}$  nucleus. This large  $|\Delta E^{oct}|$  value would suggest a stabilization of octupole deformation in the ground state. However, the experimental data do not support such a possibility [1, 81]. Non-zero octupole deformation has also been seen in RHB calculations with DD-PC1 in  $^{148,150,156}\text{Sm}$  [13].

However, the PESs are extremely soft in octupole direction in the  $^{148,156}\text{Sm}$  nuclei, so that a slightly stronger pairing (as compared with Ref. [13]) could easily drive the system to reflection symmetry. A somewhat deeper octupole minimum is seen in  $^{150}\text{Sm}$  in Ref. [13]. However, in this case the gain in binding due to octupole deformation is comparable with the one presented in Table I if the difference in pairing is taken into account. The MM calculations with a Woods-Saxon potential of Ref. [84] show that  $^{150}\text{Sm}$  is reflection symmetric in the ground state, while the ones with a folded Yukawa potential (Ref. [51] and Table I) suggests that this nucleus is only soft in octupole direction ( $|\Delta E^{oct}| = 20$  keV). The HF+BCS calculations with the Gogny force D1S of Ref. [86] predict octupole deformation in the  $N = 86 - 88$   $^{148-150}\text{Sm}$  nuclei. On the contrary, the HFB calculations with D1S and D1M forces predict octupole deformation only in  $^{150}\text{Sm}$  [71]. However, the gain in binding due to octupole deformation is small (204 keV for D1S and 43 keV for D1M).

### V. THE IMPACT OF PAIRING ON THE RELATIVE ENERGIES OF MINIMA WITH AND WITHOUT OCTUPOLE DEFORMATION.

The extrapolation beyond the known region of nuclei is always accompanied with a number of uncertainties related to the theoretical description of finite nuclei. For example, some of them are connected with the uncertainties in the theoretical description of single-particle energies [54, 55, 87, 88]; they emerge from the particle-hole channel of the density functional theories (DFTs). To some degree, these uncertainties can be estimated by using a set of different functionals as it is done in the present manuscript. In addition, there are the uncertainties in the particle-particle (pairing) channel which become especially large in the vicinity of two-neutron drip



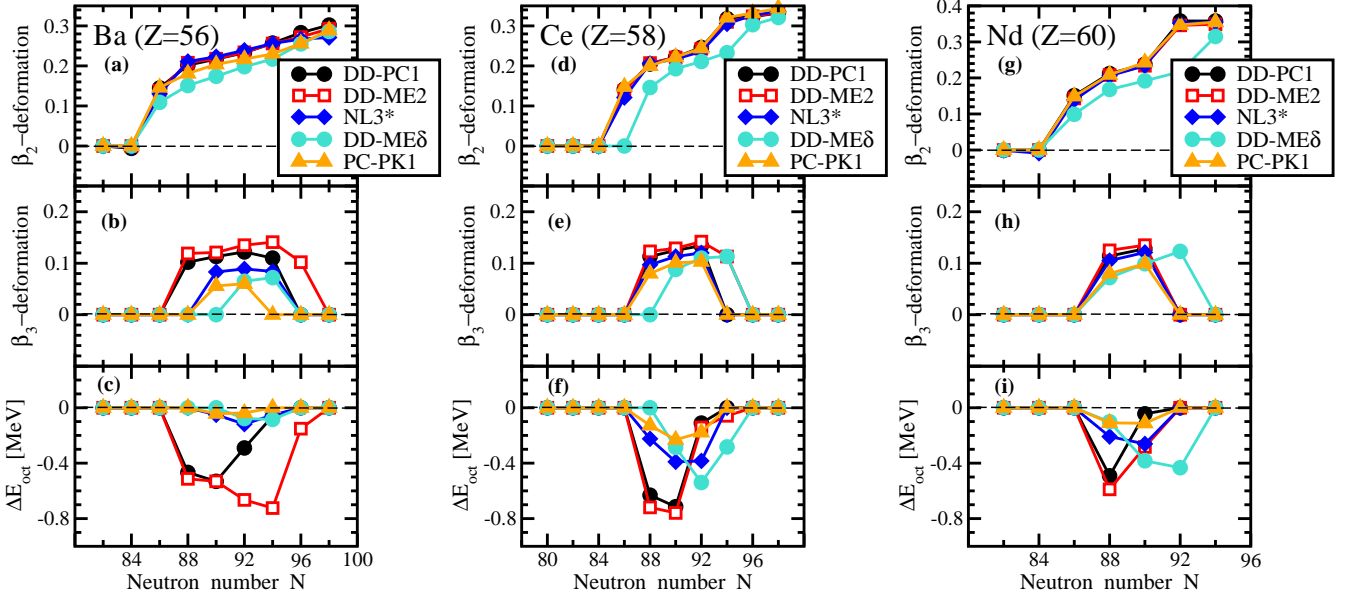


FIG. 13. (Color online) The same as Fig. 3, but for the Ba, Ce, and Nd isotopes.

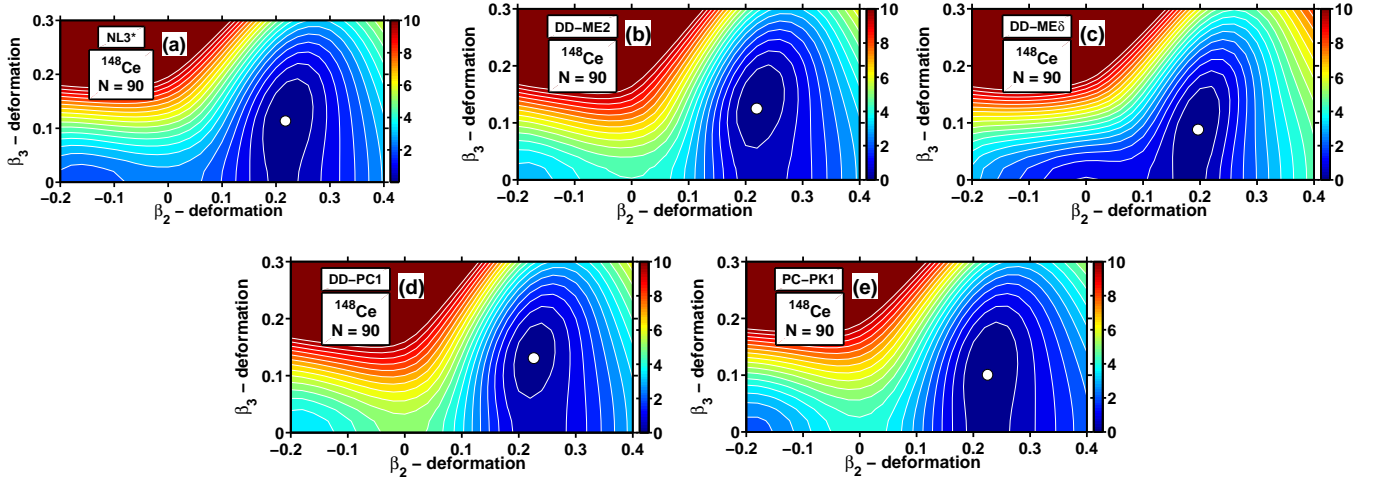


FIG. 14. (Color online) The same as Fig. 1, but for the  $^{148}\text{Ce}$  obtained with the indicated CEDFs

line (see Refs. [55, 89]). It is also expected that they can affect the relative energies of the minima with and without octupole deformation and possibly the topology of the potential energy surfaces in the cases of very soft PESs. For example, it is well known that the selection of the pairing force and the pairing strength affects the potential energy surfaces of fissioning nuclei and their fission barriers (see Ref. [65] and references therein). Moreover, as shown in this reference, fission barrier heights decrease with increasing pairing strength.

In order to understand how the variation of pairing strength affects the potential energy surfaces and relative energies of minima with and without octupole deformation in octupole soft nuclei we have performed RHB calculations with different values of the scaling factor  $f$

in Eq. (9) for the pairing force. The results of these calculations are summarized in Figs. 15 and 16.

The impact of the pairing strength on the topology of the PESs is shown in Fig. 15. Two local minima with  $\beta_2 \sim 0.05, \beta_3 = 0.0$  (further on called quadrupole minimum) and  $\beta_2 \sim 0.15, \beta_3 \sim 0.12$  (further on called octupole minimum) exist for all values of the scaling factor  $f$ . Although in this case the topology of the PES is not strongly affected by the change of  $f$ , two important features are seen. First, similar to fissioning nuclei (Ref. [65]) the barrier between quadrupole and octupole minima decreases with the increase of pairing strength. Second, the increase of pairing strength changes the relative energies of octupole and quadrupole minima. The octupole minimum is the lowest in energy for the val-

ues of  $f = 1.00, 1.03$  and  $1.06$ . However, the energy difference  $|\Delta E^{oct}|$  between these two minima decreases with increasing scaling factor  $f$ . It is well known that strong pairing favors spherical configurations. This leads to the fact that at  $f = 1.075$  pairing is so strong that the quadrupole minimum becomes spherical; this minimum is also the lowest in energy.

Similar effects are seen in more systematic investigations presented in Fig. 16 for the chain of the Th isotopes. The largest values for  $|\Delta E^{oct}|$  are always observed for the weakest pairing. This result does not depend on the functional under consideration. Thus, one can conclude that in general pairing counteracts the shell effects and favors the shapes with no octupole deformation. Or vice versa, the strongest impact of the octupole deformation (as quantified by  $\Delta E^{oct}$ ) is expected in the systems with no pairing. Note also that the variation of pairing strength typically does not affect the neutron number at which the maximum gain due to octupole deformation takes place (at  $N = 136$  for DD-PC1 and at  $N = 138$  in NL3\*).

Note that the simple analysis within the random phase approximation presented in Sec. IIIA of Ref. [1] also indicates that pairing has a tendency to make the system less octupole deformed.

## VI. CONSEQUENCES FOR ROTATIONAL NUCLEI

In Ref. [69] a systematic investigation of rotational properties of the actinides within the cranked relativistic Hartree-Bogoliubov approach with approximate particle number projection by means of the Lipkin-Nogami method (further CRHB+LN) has revealed in light even-even actinides with neutron number  $N \leq 146$  ranging from  $^{230}\text{Th}$  up to  $^{240}\text{Pu}$  a paired band crossing leading to an upbend in the kinematic moment of inertia  $J^{(1)}$  at a rotational frequency  $\Omega_x \sim 0.2$  MeV (see Figs. 9 and 10 in Ref. [69]). However, this upbend in  $J^{(1)}$  is absent in the experiment. Note that such problems with the description of rotational properties of light actinides exists in all cranking calculations (see Sec. IV of Ref. [69] for details). On the contrary, no such problems exist in the description of the band crossings in even-even actinides with neutron number  $N \geq 148$  within the CRHB+LN approach (Ref. [69]); for these nuclei this approach has also a good predictive power (Refs. [90, 91]).

The problem in the description of rotational properties of the  $N \leq 146$  actinides in Ref. [69] is most likely related to the stabilization of octupole deformation at high spin which is not taken into account in these model calculations. The arguments in favor of such an interpretation have been reviewed in Sec. IV of Ref. [69]. In particular, stable octupole deformation has been shown to delay alignment processes [92] and this may explain the differences between theory and experiment in light actinides.

The analysis of the PES of the nuclei with  $N \sim 146$  indicates that such a scenario is possible. This is illustrated by the examples of the U and Pu isotopes presented in Figs. 17 and 18. One can see that the PESs of the  $N \leq 146$  U isotopes are very soft in  $\beta_3$  direction. The octupole deformed solution with  $\beta_3 \neq 0.0$  is even the lowest in energy in  $^{238}\text{U}$ . However, the gain of binding due to octupole deformation  $|\Delta E^{oct}|$  in this nuclei is very small - only 94 keV (see Table I), and, thus, this nucleus remains in the octupole vibrational regime. Dependent on the underlying single-particle structure and its evolution with spin, the rotation of these octupole soft nuclei may lead to a stabilization of octupole deformation at high spin [73, 84, 93] and the analysis of experimental data on the  $N \leq 146$  actinides (see Sec. IV in Ref. [69]) strongly points to such a possibility. The stiffness of the PES in the direction of octupole deformation increases with the increase of neutron number above  $N = 146$  (see panels for  $^{240}\text{U}$  and  $^{242}\text{U}$  in Fig. 17). As a result, the stabilization of octupole deformation at high spin due to rotation in these two nuclei is not likely. Indeed, the predictions of the CRHB+LN calculations with no octupole deformation [69] for rotational properties of the ground state band in  $^{240}\text{U}$  almost coincide with recent experimental data [91].

The same transition from octupole soft to octupole stiff potential energy surfaces is observed between  $N = 146$  and  $N = 148$  also in Pu (see Fig. 18), Th and Cm isotopes. Fig. 18 also illustrates that the results almost do not depend on the functional since the PES obtained with DD-PC1 and NL3\* are very similar. The potential energy surfaces of the  $N = 144$  isotones (Figs. 17 and 18) are soft in  $\beta_3$  direction but the minimum of the PES is located at  $\beta_3 = 0$  (see also Table I). The same softness is observed in the  $N = 146$  isotopes (Figs. 17 and 18) but the local minimum is located at  $\beta_3 \neq 0$  (see Table I). However, the binding energy gains due to octupole deformation remain small (around 100 keV, see Table I) so that the  $N = 146$  Th, U, Pu and Cm isotopes remain in the octupole vibrational regime. On the contrary, the  $N = 148$  Th, U, Pu and Cm isotones are characterized by PES which are stiff in  $\beta_3$ -deformation (see, for example, Figs. 17 and 18).

A detailed investigation of the impact of octupole deformation on rotational properties requires the development of a symmetry unrestricted cranked RHB code which is definitely beyond the scope of the present manuscript. However, the analysis of octupole softness in the ground states establish a clear correlation with the CRHB+LN results presented in Ref. [69]. The  $N \geq 148$  actinides are characterized by PESs which are stiff in the direction of octupole deformation. As a result, no stabilization of octupole deformation due to rotation is expected in these nuclei and the experimental data on ground state rotational bands are well described in the CRHB+LN calculations with no octupole deformation [69, 90, 91]. On the contrary, the PESs of the  $N \leq 146$  actinides are soft in octupole deformation. Thus, at low

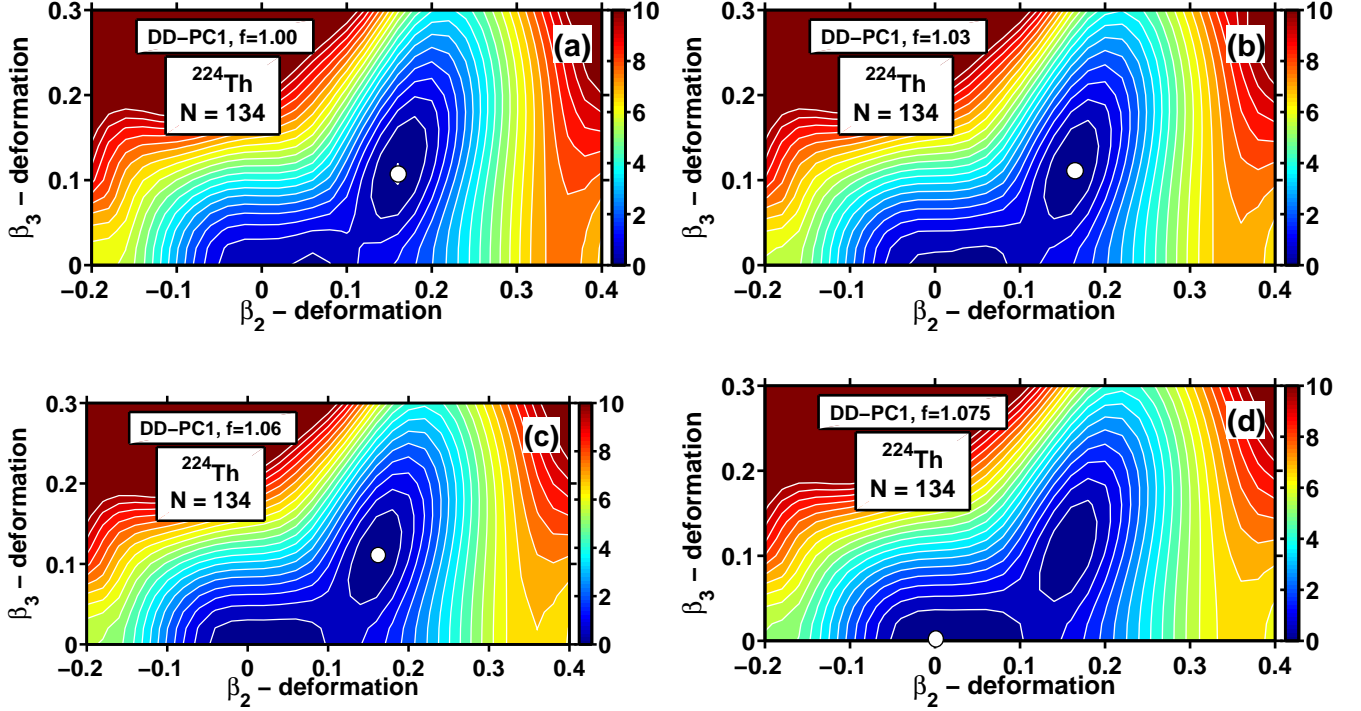


FIG. 15. (Color online) Potential energy surfaces of  $^{224}\text{Th}$  in the  $(\beta_2, \beta_3)$  plane calculated with the CEDF DD-PC1 for different values of scaling factor  $f$  of the pairing strength. White circle indicates the global minimum. Equipotential lines are shown in steps of 0.5 MeV.

spin these nuclei are in the octupole vibrational regime in which the CRHB+LN calculations with no octupole deformation describe well the moments of inertia (see Figs. 9 and 10 in Ref. [69]). However, with increasing spin the transition to static octupole deformation (or to the aligned vibrational limit) quite likely takes place and the CRHB+LN calculations of Ref. [69] with no octupole deformation could not properly describe this process; they predict upbends in the kinematic moments of inertia  $J^{(1)}$  which are not observed in experiment.

## VII. GLOBAL ANALYSIS

We have carried out a global search for octupole deformation, which covers all even-even  $Z \leq 106$  nuclei between the two-proton and two-neutron lines, with CEDFs DD-PC1 and NL3\*. The selection of these two functionals is guided by the following reasons. First, the DD-ME $\delta$  functional is omitted from global studies since it does not reproduce the experimental situation in octupole deformed actinides (Sec. III) and provides unrealistically low fission barriers in superheavy nuclei (see Ref. [94]). Second, the systematic studies with all four functionals are numerically too time-consuming to be undertaken. Thus, among the remaining functionals we selected the two functionals DD-PC1 and NL3\*, which show the largest spread of the predictions not only for octupole-

deformed nuclei (Sec. III) but also for two-neutron drip lines [54, 62], superheavy nuclei [56] and the evolution of pairing with isospin in neutron-rich nuclei [54].

The results of this search are summarized in Table I and in Fig. 19. The RHB results are also compared with the MM results of Ref. [51]. Note that the MM results cover only the part of the nuclear chart with neutron numbers  $N \leq 160$ . There are also the HFB calculations with the Gogny forces D1S, D1M and D1N [6] which cover a region of nuclei not extending far beyond the known nuclei (see Fig. 9 in Ref. [6] for details). However, these results are not added to Table I since the equilibrium octupole deformations  $\beta_3$  are not properly recorded in the supplemental material to this publication; they are always given as the multiplies of 0.02 (0.025) for the D1M (D1N and D1S) functionals which indicates that they do not correspond to the  $\beta_3$  values of the energy minimum.

One can see in Fig. 19 that in addition to the Ba, Ce and Nd isotopes as well as the actinides discussed above there are several regions of octupole deformed nuclei. These are nuclei around  $^{80}\text{Zr}$ ,  $^{110}\text{Zr}$  and  $^{200}\text{Dy}$  which are octupole soft. Since the gain of binding due to octupole deformation is quite small, no stabilization of octupole deformation is expected in these nuclei. Indeed, the interpretation of experimental data on nuclei around  $^{80}\text{Zr}$  does not require the involvement of stable octupole deformation [95]. Note that the HFB calculations with the Gogny forces also indicate octupole softness of the

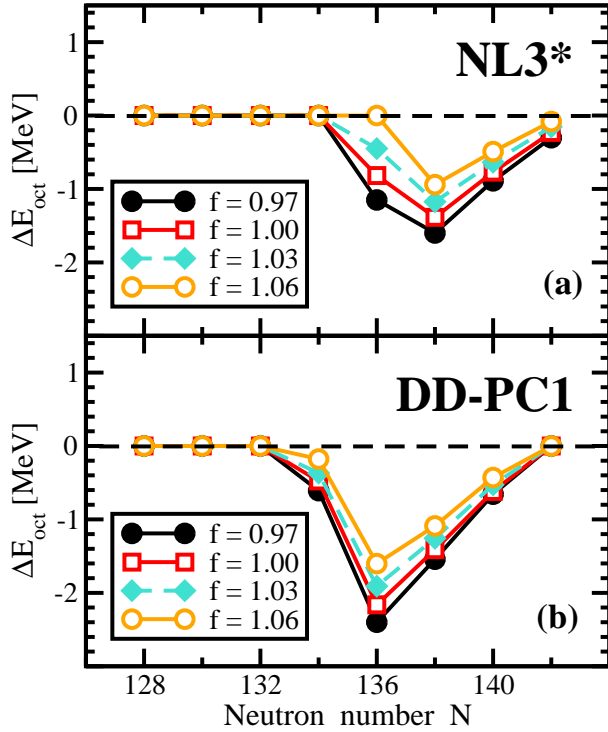


FIG. 16. (Color online). The impact of the variation of the scaling factor  $f$  of the pairing force (Eq.(9)) on the  $\Delta E_{oct}$  quantity in the  $^{218-232}\text{Th}$  isotopes. The results obtained with CEDFs NL3\* and DD-PC1 and scaling factors  $f = 0.97, 1.00, 1.03$  and  $1.06$  are presented.

nuclei around  $^{80}\text{Zr}$  (see Fig. 9 in Ref. [6]). However, in the MM calculations of Ref. [6], these nuclei do not have octupole deformation (Table I).

In the RHB calculations with DD-PC1 there exists a region of octupole soft Gd, Dy, and Er nuclei with  $N \sim 136$  and  $A \sim 200$  (Fig. 19 and Table I). However, in the RHB calculations with NL3\* octupole softness is seen only in  $^{200}\text{Dy}$ . This difference is quite likely due to the fact that pairing correlations, which counteract octupole deformation (see Sec. V), are substantially stronger in neutron-rich nuclei for the NL3\* functional as compared with DD-PC1 (Ref. [55]). This region of nuclei will not be accessible with future facilities like FRIB since it is located beyond the expected reach of FRIB (Fig. 19). As compared with our results, the MM calculations of Ref. [51] predict a much broader  $Z \sim 60, N \sim 132$  region of nuclei with non-zero octupole deformation (see Fig. 3 in Ref. [51]). Note that the HFB calculations with Gogny forces of Ref. [6] do not cover the Gd-Dy-Er region around  $A \sim 200$ .

In addition, octupole deformation is predicted in the ground states of the actinides and light superheavy nuclei with neutron number around  $N \sim 196$  (Table I and Fig. 19). To our knowledge, the existence of this region of octupole deformation, centered around  $Z \sim 98, N \sim 196$ , has not been predicted before. In many respects, it is similar to the one located in the  $Z \sim 90, N \sim 136$  ac-

tinides. For example, the gains in binding due to octupole deformation are similar in both regions and the size of these regions in the  $(Z, N)$  plane are comparable. In the center of the  $Z \sim 98, N = 196$  region,  $|\Delta E^{oct}|$  is around 1.5 MeV in the calculations with DD-PC1 and around of 1.2 MeV in the calculations with NL3\*. As a result, some of the  $N \sim 196$  actinides could have a stable octupole deformation in the ground state. This difference in  $|\Delta E^{oct}|$  could be due to the fact that pairing correlations, which counteract octupole deformation (see Sec. V), are substantially stronger in neutron-rich nuclei in the NL3\* functional as compared with DD-PC1 one (Ref. [55]).

The maximum gain in binding due to octupole deformation is changing from  $N = 198$  ( $N = 200$ ) to  $N = 192$  ( $N = 196$ ) on going from Th ( $Z = 90$ ) to Fm ( $Z = 100$ ) nuclei in the calculations with DD-PC1 (NL3\*) (see Table I). While the predictions for the location of octupole deformed nuclei in the Th-Fm region are more or less similar in the calculations with DD-PC1 and NL3\*, they diverge for the No, Rf and Sg isotopes (Fig. 19). However, this difference exists in octupole soft nuclei which have only relatively small (less than 0.6 MeV) gain in binding due to octupole deformation  $|\Delta E^{oct}|$ . It is definitely caused by the differences in underlying single-particle structure (see Ref. [56]) which also leads to different predictions for the ground state properties of superheavy nuclei (see Ref. [56] for details).

Note that this region of nuclei will not be accessible with future facilities like FRIB since it is located beyond the expected reach of FRIB (Fig. 19). However, the accounting of octupole deformation in the ground states of these nuclei is important for the modeling of fission recycling in neutron star mergers [96] since the gain in binding of the ground states due to octupole deformation will increase the fission barrier heights as compared with the case when octupole deformation is neglected.

The presence of octupole deformation in these nuclei is due to the interaction of the normal-parity  $2h_{11/2}$  (from the  $N = 7$  shell) and the intruder  $1k_{17/2}$  (from the  $N = 8$  shell) neutron orbitals. These orbitals, located above the  $N = 184$  shell gap, are very close in energy at the Fermi level in very heavy and superheavy nuclei in many nuclear potentials (see, for example, Fig. 6.9 in Ref. [97] and Fig. 1 in Ref. [56]). The octupole coupling between proton  $1i_{13/2}$  and  $2f_{7/2}$  orbitals is still active in these nuclei but its maximum is around  $Z = 98$ . On the contrary, it has a maximum around  $Z = 92$  in the  $A \sim 230$  octupole deformed actinides. This change in the position of the maximum of octupole interaction in the proton subsystem is due to the increase of the neutron excess on going from  $N \sim 136$  to  $N \sim 196$  and related modifications of the properties of the proton potential.

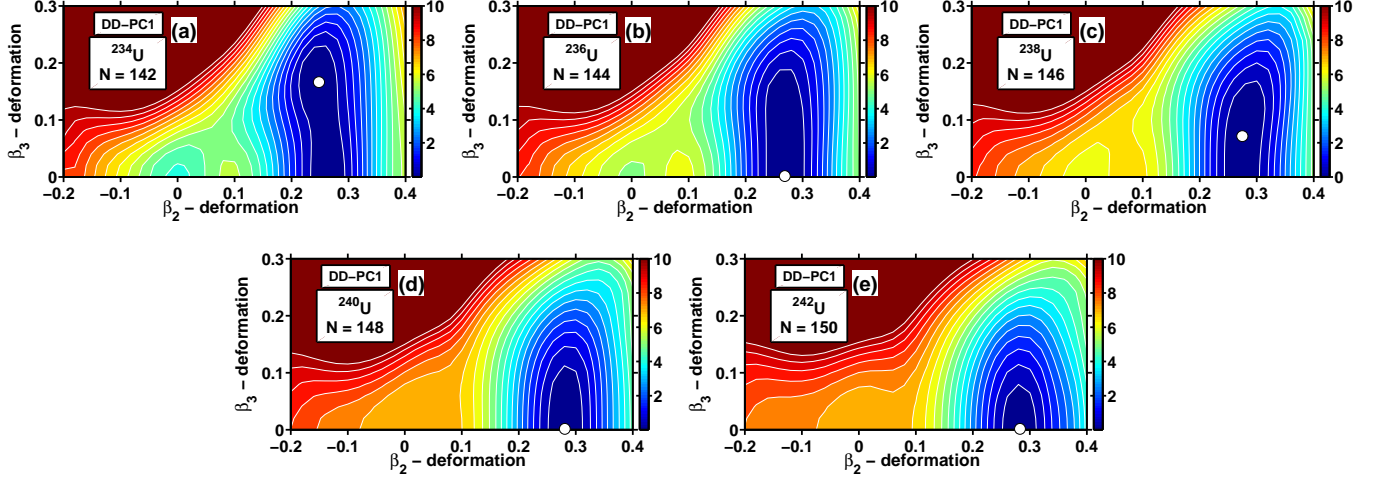


FIG. 17. (Color online) The same as Fig. 1, but for the U isotopes with  $N = 142 - 150$  calculated with the DD-PC1 functional.

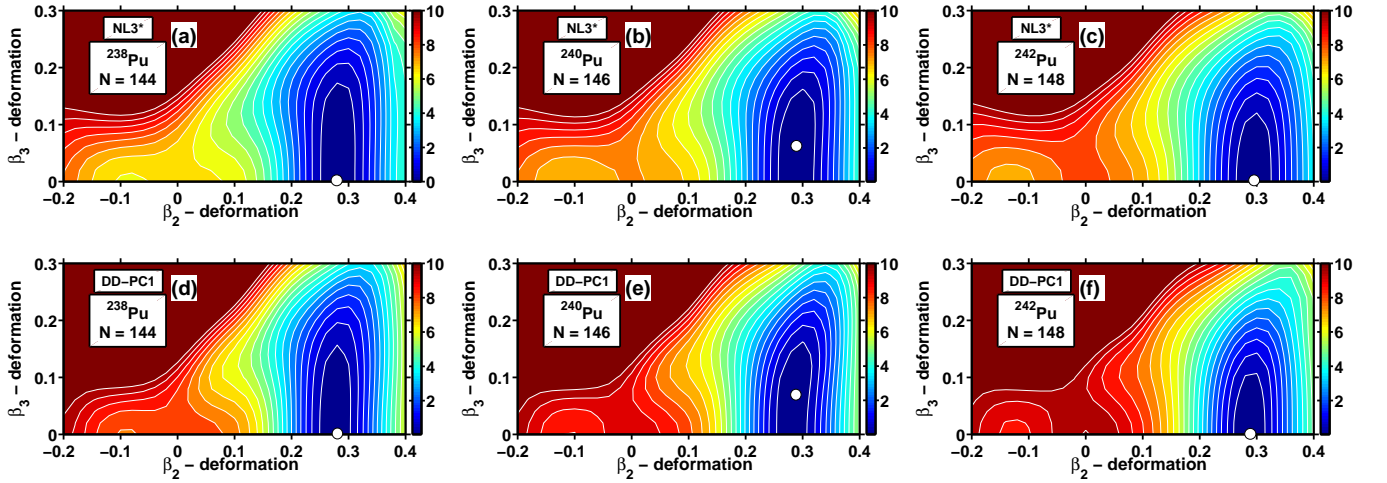


FIG. 18. (Color online) The same as Fig. 1, but for the  $N = 144 - 148$  Pu isotopes calculated with the NL3\* (upper panels) and DD-PC1 (bottom panels) functionals.

## VIII. CONCLUSIONS

A global search for octupole deformation has been performed within covariant density functional theory employing the DD-PC1 and NL3\* functionals; this search covers all even-even nuclei with  $Z \leq 106$  located between the two-neutron and two-proton drip lines. In the regions of octupole deformed light lanthanides and actinides, additional studies have been performed with the CEDFs DD-ME2, DD-ME $\delta$ , and PC-PK1 in order to establish the sensitivity of the results to the choice of the functional and to estimate theoretical uncertainties. The main results can be summarized as follows:

- The RHB calculations with the DD-PC1, PC-PK1 and DD-ME2 functionals correctly predict the islands of octupole deformation in the light lan-

thanides and actinides which in general agrees with available experimental data. The NL3\* tends to place the centers (in the  $(Z, N)$  plane) of these two islands by two neutrons higher than in above mentioned functionals. The DD-ME $\delta$  functional fails to describe experimental data in the actinides.

- The gain in binding due to octupole deformation  $|\Delta E^{oct}|$  is the quantity which defines the location and the extend of the islands of octupole deformation. If one excludes the DD-ME $\delta$  functional, theoretical uncertainties in its prediction are typically around 0.5 MeV; however, in some nuclei they reach 1 MeV. This leads to the differences in the predictions of the islands of octupole deformation. The most important source of these uncertainties is the difference in the prediction of underlying single-particle structure (see Ref. [99] for comparison of



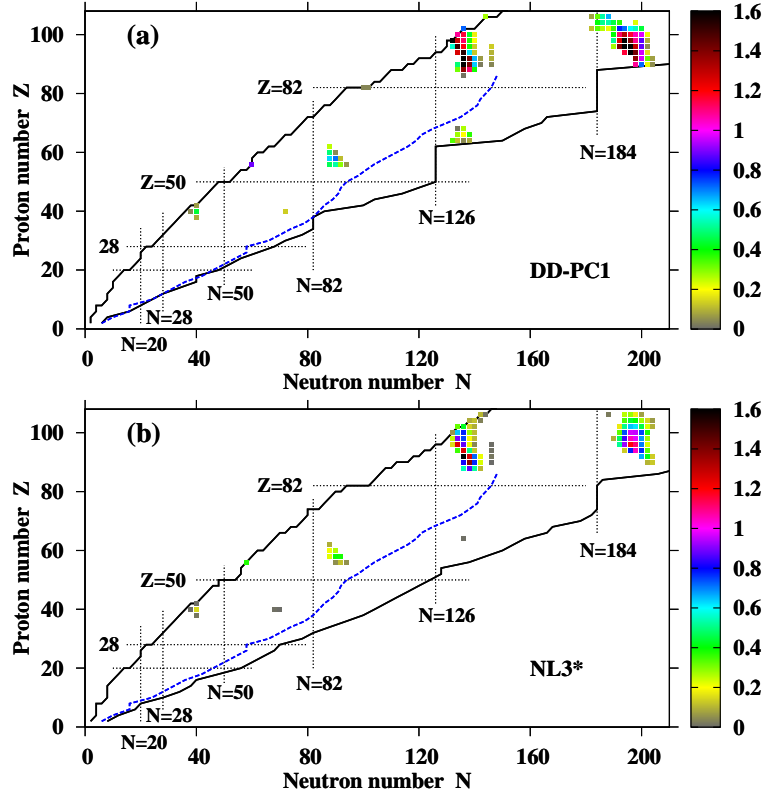


FIG. 19. (Color online) Octupole deformed nuclei in the nuclear chart. Only nuclei with non vanishing  $\Delta E^{oct}$  are shown by squares; the colors of the squares represent the values of  $|\Delta E^{oct}|$  (see colormap). Top and bottom panels display the results obtained with the CEDFs DD-PC1 and NL3\*, respectively. The blue dashed line shows the limits of the nuclear chart (defined as fission yield greater than  $10^6$ ) which may be achieved with dedicated existence measurements at FRIB [98]. The two-proton and two-neutron drip lines are displayed by solid black lines.

different DFTs). This is clearly seen for example in light lanthanides where the maximum gain in binding due to octupole deformation is located mostly at  $N = 88$  and  $N = 90$  in non-relativistic and relativistic models, respectively (see Sec. IV). Another example is the differences in the predictions of the borderlines of the island of octupole deformed nuclei in the U, Pu, Cm, Cf and Fm isotopes in relativistic and non-relativistic theories (see Sec. III).

- A new region of octupole deformation, centered around  $Z \sim 98, N \sim 196$ , has been predicted for the first time. In terms of the size in the  $(Z, N)$  plane and the impact of octupole deformation on binding energies this region is similar to the known  $Z \sim 90, N \sim 136$  region of octupole deformation in actinides. The presence of octupole deformation in these nuclei is due to the interaction of the  $2h_{11/2}$  and  $1k_{17/2}$  neutron orbitals and of the  $1i_{13/2}$  and  $2f_{7/2}$  proton orbitals. Note that the maximum of the interaction of proton orbitals occurs at a higher proton number  $Z$  as compared with the well known  $A \sim 230$  region of octupole deformation in actinides.
- Important correlations between the softness of the

potential energy surfaces in octupole deformation and the behavior of ground state rotational bands of the  $N \geq 140$  even-even nuclei have been revealed. These nuclei do not possess stable octupole deformation in the ground states. The rotational properties of the  $N \geq 148$  nuclei with stiff potential energy surfaces with respect to octupole deformation are well described in the CRHB+LN approach neglecting octupole deformation [69]. In addition, for these nuclei this approach has a predictive power as illustrated in Refs. [90, 91]. The moments of inertia of lighter nuclei are also well described at low and medium spins but the CRHB+LN approach predicts paired band crossings at rotational frequency  $\Omega_x \sim 0.2$  MeV which are not observed in experiment. This discrepancy between theory and experiment is most likely due to stabilization of octupole deformation at high spin which becomes possible because the potential energy surfaces of the  $N \leq 146$  actinides are soft in octupole deformation at the ground states.

- The impact of pairing correlations on the properties of octupole deformed nuclei has been studied. In general, pairing counteracts shell effects and fa-

vors shapes with no octupole deformation. Thus, the strongest impact of octupole deformation is expected in systems with no or weak pairing. The barrier between quadrupole and octupole local minima is at maximum for no pairing and decreases with increasing pairing strength.

- Comparing different functionals, one can see that the results obtained with the covariant energy density functional DD-ME $\delta$  differ substantially from the results of other functionals. This effect is especially pronounced in actinides where DD-ME $\delta$  does not lead to octupole deformation of the nuclei which are known to be octupole deformed. In addition, the heights of the inner fission barriers in superheavy nuclei with  $Z = 112 - 116$  obtained in this functional are significantly lower than the experimental estimates and the values calculated in all other models [94]. This functional is different from all the other functionals used here, because it has been adjusted in Ref. [61] using only four phe-

nomenological parameters in addition to some input from ab initio calculations [100, 101]. All these facts suggest that either the ab initio input for this functional is not precise enough or the number of only four phenomenological parameters (fitted to masses of spherical nuclei) is too small to provide a proper description of the details of the single-particle structure. Thus, this functional is not recommended for future investigations, in spite of the fact that it provides a good description of masses and some other ground-state observables [54].

## IX. ACKNOWLEDGEMENTS

This material is based upon work supported by the U.S. Department of Energy, Office of Science, Office of Nuclear Physics under Award Number de-sc0013037 and by the DFG cluster of excellence “Origin and Structure of the Universe” ([www.universe-cluster.de](http://www.universe-cluster.de)).

TABLE I: Calculated effect of reflection asymmetry on nuclear ground state properties. For each functional or model, the equilibrium quadrupole ( $\beta_2$ ) and octupole ( $\beta_3$ ) deformations as well as the gains in binding energy due to octupole deformation  $|\Delta E^{oct}|$  are given. The results are presented only in the case when the octupole deformed minimum is the lowest in energy. Note that  $\epsilon_2$  and  $\epsilon_3$  are the quadrupole and octupole deformations (in the Nilsson perturbed-spheroid parametrization) obtained in the MM approach of Ref. [51].

$Z(\text{Nucleus})$	$N$	$A$	DD-PC1			NL3*			mic+mac		
			$\beta_2$	$\beta_3$	$ \Delta E^{oct} $	$\beta_2$	$\beta_3$	$ \Delta E^{oct} $	$\epsilon_2$	$\epsilon_3$	$ \Delta E^{oct} $
20(Ca)	36	56							-0.07	0.02	0.04
	40	60							0.00	0.07	0.03
38(Sr)	40	78	0.005	0.084	0.089	0.005	0.078	0.019			
40(Zr)	38	78	0.003	0.068	0.043	0.003	0.060	0.005			
	40	80	0.008	0.145	0.439	0.007	0.139	0.149			
	68	108				0.002	0.060	0.009			
	70	110				0.001	0.053	0.004			
	72	112	-0.003	0.094	0.133						
42(Mo)	40	82	-0.001	0.078	0.070	-0.001	0.064	0.007			
48(Cd)	42	90							-0.01	0.04	0.04
54(Xe)	54	108							0.15	0.05	0.05
	56	110							0.16	0.07	0.20
	58	112							0.18	0.07	0.14
56(Ba)	88	142							0.13	0.06	0.11
	90	144							0.15	0.07	0.11
	52	108							0.13	0.05	0.05
	54	110							0.17	0.09	0.34
	56	112	0.244	0.114	0.284	0.274	0.188	0.792	0.18	0.10	0.48
	58	114	0.252	0.097	0.157	0.267	0.155	0.374	0.20	0.09	0.31
	60	116	0.275	0.074	0.888						

*Continued on next page*

TABLE I – *Continued from previous page*

			DD-PC1			NL3*			mic+mac		
$Z(\text{Nucleus})$	$N$	$A$	$\beta_2$	$\beta_3$	$ \Delta E^{oct} $	$\beta_2$	$\beta_3$	$ \Delta E^{oct} $	$\epsilon_2$	$\epsilon_3$	$ \Delta E^{oct} $
58(Ce)	86	142							0.12	0.06	0.14
	88	144	0.201	0.101	0.467				0.15	0.09	0.49
	90	146	0.216	0.112	0.531	0.202	0.083	0.051	0.16	0.09	0.47
	92	148	0.232	0.122	0.290	0.216	0.089	0.118			
	94	150	0.254	0.114	0.061	0.230	0.084	0.053			
	56	114	0.254	0.100	0.166	0.286	0.161	0.396	0.21	0.08	0.21
	86	144							0.13	0.07	0.22
	88	146	0.205	0.113	0.631	0.194	0.097	0.224	0.16	0.09	0.46
	90	148	0.222	0.125	0.714	0.215	0.113	0.390	0.19	0.07	0.02
	92	150	0.246	0.134	0.111	0.236	0.120	0.384			
60(Nd)	86	146							0.14	0.06	0.08
	88	148	0.206	0.114	0.491	0.198	0.105	0.208	0.18	0.06	0.09
	90	150	0.235	0.128	0.044	0.231	0.121	0.261			
62(Sm)	88	150	0.211	0.098	0.253	0.206	0.091	0.091	0.19	0.04	0.02
64(Gd)	132	196	0.136	0.062	0.335						
	134	198	0.167	0.090	0.117						
	136	200	0.192	0.119	0.046	0.182	0.003	0.008			
	138	202	0.217	0.142	0.088						
66(Dy)	134	200	0.176	0.049	0.274						
	136	202	0.202	0.090	0.200						
	138	204	0.231	0.106	0.368						
68(Er)	130	198							0.06	0.05	0.10
	132	200							0.11	0.04	0.05
	134	202	0.170	0.004	0.017				0.11	0.06	0.04
	136	204	0.200	0.065	0.265						
70(Yb)	134								0.11	0.04	0.04
76(Os)	134								0.09	0.02	0.02
78(Pt)	136								0.09	0.03	0.03
80(Hg)	136								0.06	0.05	0.02
	138								0.08	0.05	0.14
82(Pb)	98	180							0.00	0.03	0.02
	100	182	0.004	0.041	0.038				0.01	0.02	0.08
	102	184	0.002	0.041	0.038				0.00	0.02	0.04
	134	216							0.01	0.04	0.02
	136	218							0.01	0.06	0.16
	138	220							0.01	0.07	0.23
	140	222							0.01	0.07	0.26
84(Po)	134	218							0.05	0.09	0.44
	136	220							0.09	0.09	0.42
	138	222							0.10	0.08	0.16
86(Rn)	132	218							0.07	0.10	0.67
	134	220							0.10	0.09	0.85
	136	222							0.10	0.09	0.64
	138	224							0.13	0.08	0.29

*Continued on next page*

TABLE I – *Continued from previous page*

			DD-PC1			NL3*			mic+mac		
$Z(\text{Nucleus})$	$N$	$A$	$\beta_2$	$\beta_3$	$ \Delta E^{oct} $	$\beta_2$	$\beta_3$	$ \Delta E^{oct} $	$\epsilon_2$	$\epsilon_3$	$ \Delta E^{oct} $
88(Ra)	140	226							0.15	0.04	0.09
	146	232							0.21	0.02	0.02
	130	218							0.07	0.09	0.59
	132	220							0.10	0.09	1.20
	134	222	0.160	0.104	0.310				0.11	0.10	1.27
	136	224	0.177	0.125	1.370	0.178	0.124	0.547	0.13	0.10	0.91
	138	226	0.196	0.133	1.110	0.197	0.134	0.874	0.15	0.08	0.40
	140	228	0.208	0.123	0.385	0.208	0.126	0.526	0.16	0.06	0.08
	142	230				0.225	0.098	0.105			
90(Th)	130	220							0.08	0.10	1.33
	132	222							0.10	0.10	1.35
	134	224	0.167	0.112	0.491				0.13	0.11	1.22
	136	226	0.186	0.137	1.999	0.187	0.134	0.814	0.14	0.10	0.50
	138	228	0.214	0.154	1.402	0.212	0.150	1.387	0.16	0.08	0.08
	140	230	0.224	0.152	0.642	0.223	0.149	0.770			
	142	232	0.234	0.141	0.025	0.236	0.138	0.231			
	146	236	0.261	0.054	0.039	0.274	0.041	0.002			
	198	288	0.176	0.127	1.084						
92(U)	200	290	0.189	0.135	0.716						
	202	292	0.205	0.113	0.216	0.182	0.095	0.102			
	204	294	0.221	0.065	0.051	0.198	0.090	0.126			
	128	220							0.05	0.08	0.08
	130	222							0.09	0.10	1.21
	132	224							0.12	0.10	1.22
	134	226							0.13	0.10	0.60
	136	228	0.201	0.155	1.724	0.201	0.151	1.813			
	138	230	0.229	0.170	1.399	0.228	0.165	1.264			
94(Pu)	140	232	0.238	0.169	0.659	0.238	0.166	0.721			
	142	234	0.245	0.170	0.067	0.247	0.162	0.217			
	146	238	0.275	0.078	0.094	0.284	0.068	0.019			
	198	290	0.181	0.140	1.378						
	200	292	0.196	0.151	0.969	0.183	0.124	0.664			
	202	294	0.214	0.137	0.319	0.200	0.127	0.416			
	204	296	0.233	0.082	0.074	0.220	0.117	0.133			
	128	222							0.05	0.08	0.35
	130	224							0.09	0.10	1.09
96(Cm)	132	226							0.12	0.10	0.59
	134	228	0.170	0.134	1.260	0.167	0.129	0.354	0.14	0.10	0.04
	136	230	0.197	0.155	1.535	0.196	0.152	1.251			
	138	232	0.246	0.161	0.622	0.240	0.159	0.501			
	140	234	0.263	0.133	0.125	0.261	0.142	0.121			
	146	240	0.284	0.066	0.099	0.290	0.054	0.010			
	194	288	0.131	0.108	1.156	0.119	0.089	0.132			
	196	290	0.156	0.131	1.774	0.151	0.118	0.780			
	198	292	0.176	0.146	1.419	0.171	0.135	1.046			
96(Cm)	200	294	0.192	0.158	0.965	0.187	0.142	0.770			
	202	296	0.216	0.141	0.162	0.206	0.143	0.327			
	128	224							0.04	0.08	0.52
	130	226							0.08	0.10	0.84
	132	228	0.134	0.115	0.562	0.130	0.111	0.152	0.14	0.08	0.02
	134	230	0.162	0.135	1.511	0.159	0.132	1.248			

*Continued on next page*

TABLE I – *Continued from previous page*

			DD-PC1			NL3*			mic+mac					
Z(Nucleus)	N	A	$\beta_2$	$\beta_3$	$ \Delta E^{oct} $	$\beta_2$	$\beta_3$	$ \Delta E^{oct} $	$\epsilon_2$	$\epsilon_3$	$ \Delta E^{oct} $			
98(Cf)	136	232	0.195	0.158	1.190	0.194	0.154	0.877						
	138	234	0.252	0.142	0.387	0.249	0.145	0.212						
	140	236	0.274	0.098	0.131	0.275	0.096	0.041						
	146	242	0.295	0.063	0.132	0.298	0.044	0.005						
	190	286	0.095	0.105	0.271									
	192	288	0.115	0.116	1.394									
	194	290	0.131	0.126	1.994									
	196	292	0.150	0.137	1.790									
	198	294	0.170	0.151	1.294									
	200	296	0.190	0.164	0.878									
	202	298	0.217	0.142	0.049									
	126	224	0.008	0.065	0.151									
	128	226	0.015	0.049	0.032									
	130	228												
	132	230										0.146	0.111	0.427
	134	232										0.172	0.141	1.292
136	234	0.198				0.164	1.122							
138	236	0.245	0.146	0.379	0.244	0.146	0.195							
140	238	0.266	0.114	0.197	0.266	0.114	0.107							
100(Fm)	190	288	0.106	0.123	0.515	0.102	0.090	0.095						
	192	290	0.131	0.131	1.259	0.132	0.114	0.473						
	194	292	0.146	0.140	1.632	0.153	0.134	0.848						
	196	294	0.164	0.150	1.388	0.171	0.152	1.056						
	198	296	0.180	0.162	1.087	0.185	0.162	0.983						
	200	298	0.196	0.173	0.868	0.199	0.168	0.680						
	202	300	0.218	0.147	0.094	0.217	0.164	0.273						
	126	226	0.011	0.089	0.490	0.014	0.085	0.207						
	128	228	0.014	0.079	0.149	0.023	0.073	0.092						
	132	232	0.161	0.085	0.152	0.164	0.095	0.061						
	134	234	0.187	0.146	1.084	0.188	0.145	0.646						
	136	236	0.201	0.172	1.156	0.202	0.166	0.774						
	138	238	0.226	0.158	0.434	0.223	0.160	0.282						
	140	240	0.258	0.110	0.177	0.253	0.122	0.110						
	102(No)	190	290	0.137	0.129	0.403								
		192	292	0.162	0.149	1.119								
194		294	0.170	0.159	1.309									
196		296	0.183	0.169	1.160									
198		298	0.195	0.177	1.056									
200		300	0.204	0.184	0.976									
202		302	0.216	0.157	0.218									
134		236				0.197	0.120	0.321						
136		238				0.206	0.144	0.424						
138		240				0.227	0.134	0.138						
140		242				0.251	0.113	0.091						
182		284	0.014	0.065	0.115									
184		286	0.007	0.085	0.334									
186		288	-0.004	0.085	0.257									
188		290	-0.033	0.082	0.214									
190		292	0.176	0.122	0.357									
192	294	0.172	0.139	0.776										
194	296	0.181	0.145	0.717										
196	298	0.194	0.152	0.602										
194	296	0.181	0.145	0.717	0.174				0.136	0.512				
196	298	0.194	0.152	0.602	0.192				0.148	0.646				

*Continued on next page*



TABLE I – *Continued from previous page*

			DD-PC1			NL3*			mic+mac		
Z(Nucleus)	N	A	$\beta_2$	$\beta_3$	$\Delta E^{oct}$	$\beta_2$	$\beta_3$	$\Delta E^{oct}$	$\epsilon_2$	$\epsilon_3$	$ \Delta E^{oct} $
104(Rf)	198	300	0.206	0.156	0.550	0.206	0.156	0.619			
	200	302	0.214	0.159	0.445	0.219	0.157	0.454			
	202	304				0.235	0.138	0.230			
	204	306				0.248	0.105	0.095			
	138	242				0.241	0.094	0.090			
	140	244				0.254	0.102	0.117			
	142	246				0.264	0.094	0.032			
	184	288	0.002	0.090	0.407						
	186	290	-0.025	0.101	0.513						
	188	292	-0.039	0.100	0.536						
106(Sg)	190	294	0.195	0.105	0.454						
	192	296	0.201	0.116	0.366						
	194	298				0.179	0.115	0.340			
	196	300	0.230	0.126	0.226	0.218	0.134	0.402			
	200	304				0.232	0.131	0.276			
	202	306				0.246	0.111	0.145			
	204	308				0.256	0.086	0.067			
	142	248				0.264	0.098	0.104			
	144	250	0.266	0.052	0.271	0.272	0.060	0.013			
	182	288	-0.003	0.055	0.076						
	184	290	-0.003	0.084	0.320						
	186	292	-0.032	0.102	0.530						
	188	294	-0.046	0.103	0.660	-0.033	0.060	0.024			
	194	300				0.182	0.097	0.257			
	196	302				0.211	0.109	0.282			
	198	304				0.230	0.111	0.179			
	200	306				0.246	0.098	0.073			

- 
- [1] P. A. Butler and W. Nazarewicz, *Rev. Mod. Phys.* **68**, 349 (1996).
- [2] H. Abusara, A. V. Afanasjev, and P. Ring, *Phys. Rev. C* **85**, 024314 (2012).
- [3] J. Erler, K. Langanke, H. P. Loens, G. Martinez-Pinedo, and P.-G. Reinhard, *Phys. Rev. C* **85**, 025802 (2012).
- [4] N. Wang, J. Meng, and E.-G. Zhao, *Comm. Th. Phys.* **53**, 1145 (2010).
- [5] J.-Y. Guo, P. Jiao, and X.-Z. Fang, *Phys. Rev. C* **82**, 047301 (2010).
- [6] L. M. Robledo and G. F. Bertsch, *Phys. Rev. C* **84**, 054302 (2011).
- [7] N. Minkov, S. Drenska, M. Strecker, W. Scheid, and H. Lenske, *Phys. Rev. C* **85**, 034306 (2012).
- [8] R. V. Jolos, P. von Brentano, and J. Jolie, *Phys. Rev. C* **86**, 024319 (2012).
- [9] H.-L. Wang, H.-L. Liu, and F.-R. Xu, *Phys. Scripta* **86**, 035201 (2012).
- [10] L. M. Robledo and R. R. Rodríguez-Guzmán, *J. Phys. G* **39**, 105103 (2012).
- [11] J. Zhao, B.-N. Lu, E.-G. Zhao, and S.-G. Zhou, *Phys. Rev. C* **86**, 057304 (2012).
- [12] K. Nomura, D. Vretenar, and B.-N. Lu, *Phys. Rev. C* **88**, 021303 (2013).
- [13] K. Nomura, D. Vretenar, T. Nikšić, and B.-N. Lu, *Phys. Rev. C* **89**, 024312 (2014).
- [14] Y.-J. Chen, Z.-C. Gao, Y.-S. Chen, and Y. Tu, *Phys. Rev. C* **91**, 014317 (2015).
- [15] K. Nomura, R. Rodríguez-Guzmán, and L. M. Robledo, *Phys. Rev. C* **92**, 014312 (2015).
- [16] H.-L. Wang, J. Yang, M.-L. Liu, and F.-R. Xu, *Phys. Rev. C* **92**, 024303 (2015).
- [17] J. M. Yao, E. F. Zhou, and Z. P. Li, *Phys. Rev. C* **92**, 041304 (2015).
- [18] T. Rzaca-Urban, W. Urban, J. A. Pinston, G. S. Simpson, A. G. Smith, and I. Ahmad, *Phys. Rev. C* **86**, 044324 (2012).
- [19] T. Rzaca-Urban, W. Urban, A. G. Smith, I. Ahmad, and A. Syntfeld-Kazuch, *Phys. Rev. C* **87**, 031305 (2013).
- [20] L. P. Gaffney, P. A. Butler, M. Scheck, A. B. Hayes, F. Wenander, M. Albers, B. Bastin, C. Bauer, A. Blazhev, S. Bönig, N. Bree, J. Cederkäll, T. Chupp, D. C. T. E. Cocolios, T. Davinson, H. D. Witte,

- J. Diriken, T. Grahn, A. Herzan, M. Huyse, D. G. Jenkins, D. T. Joss, N. K. J. Konki, M. Kowalczyk, T. Kröll, E. Kwan, R. Lutter, K. Moschner, P. Napiorkowski, J. Pakarinen, M. Pfeiffer, D. Radeck, P. Reiter, K. Reynnders, S. V. Rigby, L. M. Robledo, M. Rudigier, S. Sambhi, M. Seidlitz, B. Siebeck, T. Stora, P. Thoele, P. V. Duppen, M. J. Vermeulen, M. von Schmid, D. Voulot, N. Warr, K. Wimmer, K. Wrzosek-Lipska, C. Y. W., and M. Zielinska, *Nature* **497**, 199 (2013).
- [21] S. K. Tandel, M. Hemalatha, A. Y. Deo, S. B. Patel, R. Palit, T. Trivedi, J. Sethi, S. Saha, D. C. Biswas, and S. Mukhopadhyay, *Phys. Rev. C* **87**, 034319 (2013).
- [22] M. Spieker, D. Bucurescu, J. Endres, T. Faestermann, R. Hertenberger, S. Pascu, S. Skalacki, S. Weber, H.-F. Wirth, N.-V. Zamfir, and A. Zilges, *Phys. Rev. C* **88**, 041303 (2013).
- [23] M. Scheck, L. P. Gaffney, P. A. Butler, A. B. Hayes, F. Wenander, M. Albers, B. Bastin, C. Bauer, A. Blazhev, S. Bnig, N. Bree, J. Cederkil, T. Chupp, D. Cline, T. E. Cocolios, T. Davinson, H. D. Witte, J. Diriken, T. Grahn, E. T. Gregor, A. Herzan, M. Huyse, D. G. Jenkins, D. T. Joss, N. Kesteloot, J. Konki, M. Kowalczyk, T. Kröll, E. Kwan, R. Lutter, K. Moschner, P. Napiorkowski, J. Pakarinen, M. Pfeiffer, D. Radeck, P. Reiter, K. Reynnders, S. V. Rigby, L. M. Robledo, M. Rudigier, S. Sambhi, M. Seidlitz, B. Siebeck, T. Stora, P. Thoele, P. V. Duppen, M. J. Vermeulen, M. von Schmid, D. Voulot, N. Warr, K. Wimmer, K. Wrzosek-Lipska, C. Y. Wu, and M. Zielinska, *J. Phys.: Conf. Series* **533**, 012007 (2014).
- [24] H. J. Li, S. J. Zhu, J. H. Hamilton, E. H. Wang, A. V. Ramayya, Y. J. Chen, J. K. Hwang, J. Ranger, S. H. Liu, Z. G. Xiao, Y. Huang, Z. Zhang, Y. X. Luo, J. O. Rasmussen, I. Y. Lee, G. M. Ter-Akopian, Y. T. Oganessian, and W. C. Ma, *Phys. Rev. C* **90**, 047303 (2014).
- [25] I. Ahmad, R. R. Chasman, J. P. Greene, F. G. Kondev, and S. Zhu, *Phys. Rev. C* **92**, 024313 (2015).
- [26] E. Ruchowska, H. Mach, M. Kowal, J. Skalski, W. A. Plóciennik, and B. Fogelberg, *Phys. Rev. C* **92**, 034328 (2015).
- [27] H. Abusara, A. V. Afanasjev, and P. Ring, *Phys. Rev. C* **82**, 044303 (2010).
- [28] V. Prassa, T. Nikšić, G. A. Lalazissis, and D. Vretenar, *Phys. Rev. C* **86**, 024317 (2012).
- [29] B.-N. Lu, J. Zhao, E.-G. Zhao, and S.-G. Zhou, *Phys. Rev. C* **89**, 014323 (2014).
- [30] M. Warda and J. L. Egidio, *Phys. Rev. C* **86**, 014322 (2012).
- [31] N. Dubray, H. Goutte, and J.-P. Delaroche, *Phys. Rev. C* **77**, 014310 (2008).
- [32] M. Warda and L. M. Robledo, *Phys. Rev. C* **84**, 044608 (2011).
- [33] R. Rodríguez-Guzmán and L. M. Robledo, *Phys. Rev. C* **89**, 054310 (2014).
- [34] A. Staszczak, A. Baran, and W. Nazarewicz, *Phys. Rev. C* **87**, 024320 (2013).
- [35] J. Sadhukhan, K. Mazurek, A. Baran, J. Dobaczewski, W. Nazarewicz, and J. A. Sheikh, *Phys. Rev. C* **88**, 064314 (2013).
- [36] P. Möller, A. J. Sierk, T. Ichikawa, A. Iwamoto, R. Bengtsson, H. Uhrenholt, and S. Åberg, *Phys. Rev. C* **79**, 064304 (2009).
- [37] M. Kowal, P. Jachimowicz, and A. Sobieczewski, *Phys. Rev. C* **82**, 014303 (2010).
- [38] A. N. Andreyev, J. Elseviers, M. Huyse, P. Van Duppen, S. Antalic, A. Barzakh, N. Bree, T. E. Cocolios, V. F. Comas, J. Diriken, D. Fedorov, V. Fedosseev, S. Franchoo, J. A. Heredia, O. Ivanov, U. Köster, B. A. Marsh, K. Nishio, R. D. Page, N. Patronis, M. Seliverstov, I. Tsekhanovich, P. Van den Bergh, J. Van De Walle, M. Venhart, S. Vermote, M. Veselsky, C. Wagemans, T. Ichikawa, A. Iwamoto, P. Möller, and A. J. Sierk, *Phys. Rev. Lett.* **105**, 252502 (2010).
- [39] L. Csige, D. M. Filipescu, T. Glodariu, J. Gulyás, M. M. Günther, D. Habs, H. J. Karwowski, A. Krasznahorkay, G. C. Rich, M. Sin, L. Stroe, O. Tesileanu, and P. G. Thirolf, *Phys. Rev. C* **87**, 044321 (2013).
- [40] A. N. Andreyev, M. Huyse, and P. Van Duppen, *Rev. Mod. Phys.* **85**, 1541 (2013).
- [41] D. Vretenar, A. V. Afanasjev, G. A. Lalazissis, and P. Ring, *Phys. Rep.* **409**, 101 (2005).
- [42] P.-G. Reinhard, *Rep. Prog. Phys.* **52**, 439 (1989).
- [43] P. Ring, *Prog. Part. Nucl. Phys.* **37** (1996).
- [44] M. Bender, K. Rutz, P.-G. Reinhard, J. A. Maruhn, and W. Greiner, *Phys. Rev. C* **60**, 034304 (1999).
- [45] E. V. Litvinova and A. V. Afanasjev, *Phys. Rev. C* **84**, 014305 (2011).
- [46] A. V. Afanasjev and H. Abusara, *Phys. Rev. C* **81**, 014309 (2010).
- [47] K. Rutz, J. A. Maruhn, P. G. Reinhard, and W. Greiner, *Nucl. Phys. A* **590**, 680 (1995).
- [48] L. S. Geng, J. Meng, and H. Toki, *Chin. Phys. Lett.* **24**, 1865 (2007).
- [49] W. Zhang, Z.-P. Li, and S.-Q. Zhang, *Chi. Ph. C* **34**, 1094 (2010).
- [50] W. Zhang, Z. P. Li, S. Q. Zhang, and J. Meng, *Phys. Rev. C* **81**, 034302 (2010).
- [51] P. Möller, R. Bengtsson, B. Carlsson, P. Olivius, T. Ichikawa, H. Sagawa, and A. Iwamoto, *At. Data and Nucl. Data Tables* **94**, 758 (2008).
- [52] P. G. Reinhard and W. Nazarewicz, *Phys. Rev. C* **81**, 051303(R) (2010).
- [53] J. Dobaczewski, W. Nazarewicz, and P.-G. Reinhard, *J. Phys. G* **41**, 074001 (2014).
- [54] S. E. Agbemava, A. V. Afanasjev, D. Ray, and P. Ring, *Phys. Rev. C* **89**, 054320 (2014).
- [55] A. V. Afanasjev, S. E. Agbemava, D. Ray, and P. Ring, *Phys. Rev. C* **91**, 014324 (2015).
- [56] S. E. Agbemava, A. V. Afanasjev, T. Nakatsukasa, and P. Ring, *Phys. Rev. C* **92**, 054310 (2015).
- [57] T. Nikšić, D. Vretenar, and P. Ring, *Phys. Rev. C* **78**, 034318 (2008).
- [58] G. A. Lalazissis, S. Karatzikos, R. Fossion, D. P. Arteaga, A. V. Afanasjev, and P. Ring, *Phys. Lett. B* **671**, 36 (2009).
- [59] G. A. Lalazissis, T. Nikšić, D. Vretenar, and P. Ring, *Phys. Rev. C* **71**, 024312 (2005).
- [60] P. W. Zhao, Z. P. Li, J. M. Yao, and J. Meng, *Phys. Rev. C* **82**, 054319 (2010).
- [61] X. Roca-Maza, X. Viñas, M. Centelles, P. Ring, and P. Schuck, *Phys. Rev. C* **84**, 054309 (2011).
- [62] A. V. Afanasjev, S. E. Agbemava, D. Ray, and P. Ring, *Phys. Lett. B* **726**, 680 (2013).
- [63] P. Ring and P. Schuck, *The Nuclear Many-Body Problem* (Springer-Verlag, Berlin) (1980).
- [64] P. Bonche, H. Flocard, and P. H. Heenen, *Comp. Phys. Comm.* **171**, 49 (2005).

- [65] S. Karatzikos, A. V. Afanasjev, G. A. Lalazissis, and P. Ring, Phys. Lett. B **689**, 72 (2010).
- [66] Y. Tian, Z. Y. Ma, and P. Ring, Phys. Lett. B **676**, 44 (2009).
- [67] J. F. Berger, M. Girod, and D. Gogny, Comp. Phys. Comm. **63**, 365 (1991).
- [68] A. V. Afanasjev, T. L. Khoo, S. Frauendorf, G. A. Lalazissis, and I. Ahmad, Phys. Rev. C **67**, 024309 (2003).
- [69] A. V. Afanasjev and O. Abdurazakov, Phys. Rev. C **88**, 014320 (2013).
- [70] Y. K. Gambhir, P. Ring, and A. Thimet, Ann. Phys. (N.Y.) **198**, 132 (1990).
- [71] R. Rodríguez-Guzmán, L. M. Robledo, and P. Sarriguren, Phys. Rev. C **86**, 034336 (2012).
- [72] E. F. Zhou, J. Yao, Z. Li, J. Meng, and P. Ring, Phys. Lett. B **753**, 227 (2016).
- [73] E. Garrote, J. L. Egido, and L. M. Robledo, Phys. Rev. Lett. **80**, 4398 (1998).
- [74] L. M. Robledo, J. Phys. G **42**, 055109 (2015).
- [75] J. Cocks, D. Hawcroft, N. Amzal, P. Butler, K. Cann, P. Greenlees, G. Jones, S. Asztalos, R. Clark, M. Deleplanque, R. Diamond, P. Fallon, I. Lee, A. Macchiavelli, R. MacLeod, F. Stephens, P. Jones, R. Julin, R. Broda, B. Fornal, J. Smith, T. Lauritsen, P. Bhattacharyya, and C. Zhang, Nucl. Phys. A **645**, 61 (1999).
- [76] W. Nazarewicz, P. Olanders, I. Ragnarsson, J. Dudek, G. Leander, P. Mller, and E. Ruchowska, Nucl. Phys. A **429**, 269 (1984).
- [77] L. M. Robledo and P. A. Butler, Phys. Rev. C **88**, 051302 (2013).
- [78] J. Egido and L. Robledo, Nucl. Phys. A **494**, 85 (1989).
- [79] L. M. Robledo, M. Baldo, P. Schuck, and X. Viñas, Phys. Rev. C **81**, 034315 (2010).
- [80] P. T. Greenlees, N. Amzal, P. A. Butler, K. J. Cann, J. F. C. Cocks, D. Hawcroft, G. D. Jones, R. D. Page, A. Andreev, T. Enqvist, P. Fallon, B. Gall, M. Guttormsen, K. Helariutta, F. Hoellinger, P. M. Jones, R. Julin, S. Juutinen, H. Kankaanp, H. Ketunen, P. Kuusiniemi, M. Leino, S. Messelt, M. Muikku, A. Savelius, A. Schiller, S. Siem, W. H. Trzaska, T. Tveter, and J. Uusitalo, J. Phys. G **24**, L63 (1998).
- [81] Evaluated Nuclear Structure Data File (ENSDF) located at the website (<http://www.nndc.bnl.gov/ensdf/>) of Brookhaven National Laboratory. ENSDF is based on the publications presented in Nuclear Data Sheets (NDS) which is a standard for evaluated nuclear data. (2015).
- [82] X. Wang, R. V. F. Janssens, M. P. Carpenter, S. Zhu, I. Wiedenhöver, U. Garg, S. Frauendorf, T. Nakatsukasa, I. Ahmad, A. Bernstein, E. Dienderfer, S. J. Freeman, J. P. Greene, T. L. Khoo, F. G. Kondev, A. Larabee, T. Lauritsen, C. J. Lister, B. Meredith, D. Seweryniak, C. Teal, and P. Wilson, Phys. Rev. Lett. **102**, 122501 (2009).
- [83] S. Frauendorf, Phys. Rev. C **77**, 021304(R) (2008).
- [84] W. Nazarewicz and S. L. Tabor, Phys. Rev. C **45**, 2226 (1992).
- [85] V. Martín and L. M. Robledo, Phys. Rev. C **48**, 188 (1993).
- [86] J. Egido and L. Robledo, Nucl. Phys. A **545**, 589 (1992).
- [87] A. V. Afanasjev and S. Shawaqfeh, Phys. Lett. B **706**, 177 (2011).
- [88] A. V. Afanasjev, J. Phys. G **42**, 034002 (2014).
- [89] A. Pastore, J. Margueron, P. Schuck, and X. Viñas, Phys. Rev. C **88**, 034314 (2013).
- [90] A. V. Afanasjev, Phys. Scr. **89**, 054001 (2014).
- [91] B. Birkenbach, A. Vogt, K. Geibel, F. Recchia, P. Reiter, J. J. Valiente-Dobón, D. Bazzacco, M. Bowry, A. Bracco, B. Bruyneel, L. Corradi, F. C. L. Crespi, G. de Angelis, P. Désesquelles, J. Eberth, E. Farnea, E. Fioretto, A. Gadea, A. Gengelbach, A. Giaz, A. Görgen, A. Gottardo, J. Grebosz, H. Hess, P. R. John, J. Jolie, D. S. Judson, A. Jungclaus, W. Korsten, S. Lenzi, S. Leoni, S. Lunardi, R. Menegazzo, D. Mengoni, C. Michelagnoli, T. Mijatović, G. Montagnoli, D. Montanari, D. Napoli, L. Pellegri, G. Pollarolo, A. Pullia, B. Quintana, F. Radeck, D. Rosso, E. Şahin, M. D. Salsac, F. Scarlassara, P.-A. Söderström, A. M. Stefanini, T. Steinbach, O. Stezowski, S. Szilner, B. Szpak, C. Theisen, C. Ur, V. Vandone, and A. Wiens, Phys. Rev. C **92**, 044319 (2015).
- [92] S. Frauendorf and V. V. Pashkevich, Phys. Lett. B **141**, 23 (1984).
- [93] W. Nazarewicz, G. Leander, and J. Dudek, Nucl. Phys. A **467**, 437 (1987).
- [94] S. E. Agbemava, A. V. Afanasjev, T. Nakatsukasa, and P. Ring, (in preparation).
- [95] W. Nazarewicz, J. Dudek, R. Bengtsson, T. Bengtsson, and I. Ragnarsson, Nucl. Phys. A **435**, 397 (1985).
- [96] S. Goriely, A. Bauswein, and H.-T. Janka, Astr. Phys. J **738**, L32 (2011).
- [97] S. G. Nilsson and I. Ragnarsson, *Shapes and shells in nuclear structure*, (Cambridge University Press, 1995).
- [98] H. Schatz, private communication, see also <https://groups.nsl.msui.edu/frib/rates/fribrates.html> (2014).
- [99] J. Dobaczewski, A. V. Afanasjev, M. Bender, L. M. Robledo, and Y. Shi, Nucl. Phys. A **944**, 388 (2015).
- [100] M. Baldo, C. Maieron, P. Schuck, and X. Viñas, Nucl. Phys. A **736**, 241 (2004).
- [101] E. N. E. van Dalen, C. Fuchs, and A. Faessler, Eur. Phys. J. A **31**, 29 (2007).